CSDL-T-1134

ROBUST RENDEZVOUS
MANEUVER POINT CONDITIONS

by
Debra Ann Fogle

June 1992

Master of Science Thesis
Massachusetts Institute of Technology

DRAPER ◉
LABORATORY
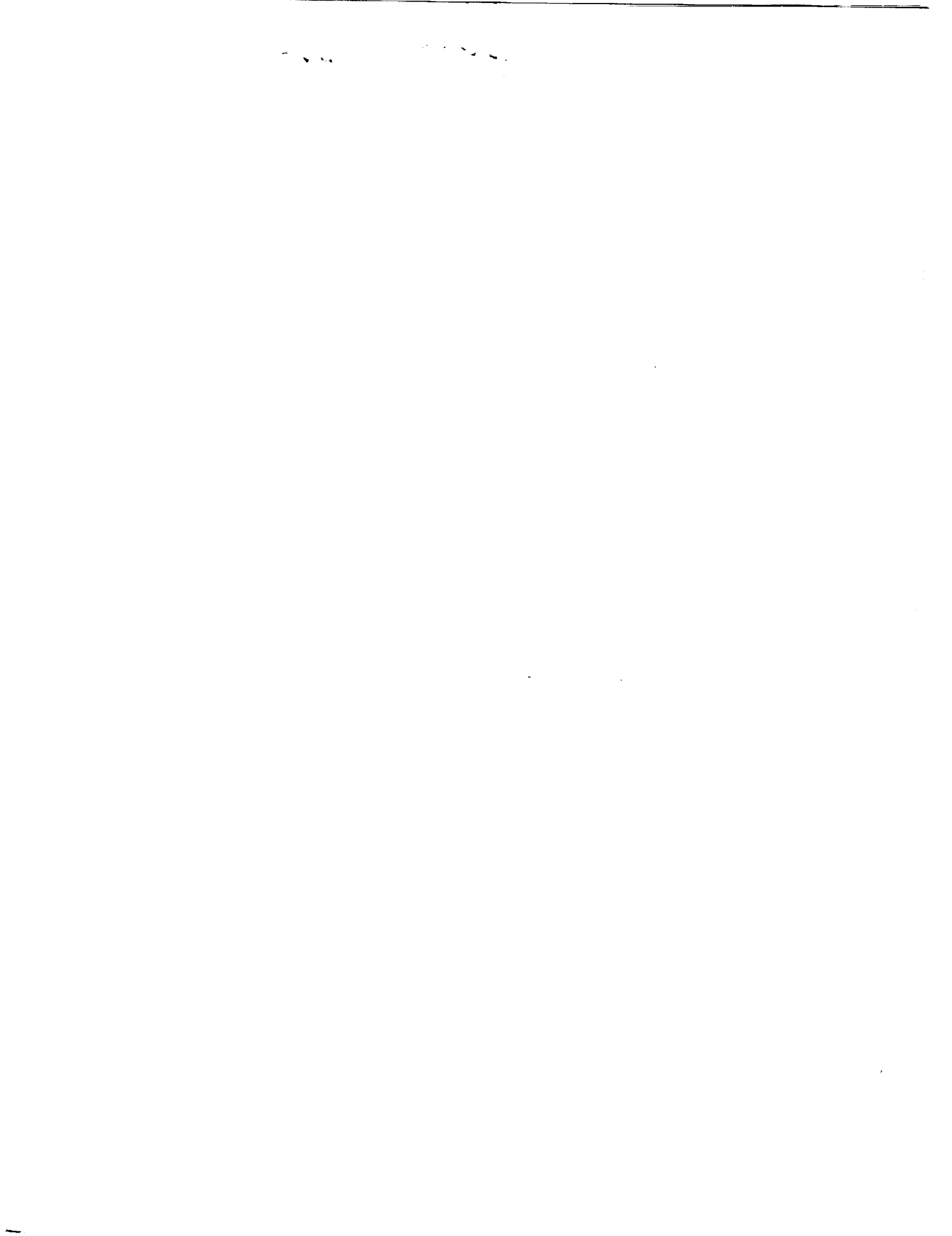
Robust Rendezvous
Maneuver Point Conditions

by

Debra Ann Fogle

B.S.A.A.E., The Ohio State University

(1986)

Submitted in Partial Fulfillment

of the Requirements for the

Degree of

Master of Science

in Aeronautics and Astronautics

at the

Massachusetts Institute of Technology

June 1992

© Debra Ann Fogle, 1992

Signature of Author _____

Department of Aeronautics and Astronautics

June 1992

Certified by _____

Professor Richard H. Battin

Thesis Supervisor, Department of Aeronautics and Astronautics

Certified by _____

Peter M. Kachmar

Technical Supervisor, Charles Stark Draper Laboratory

Certified by _____

Stanley W. Shepperd

Technical Supervisor, Charles Stark Draper Laboratory

Accepted by _____

Harold Y. Wachman

Chairman, Department Graduate Committee

1

Robust Rendezvous
Maneuver Point Conditions

by
Debra Ann Fogle

Submitted to the Department of Aeronautics and Astronautics
on May 15, 1992
in partial fulfillment of the requirements for the degree of
Master of Science in Aeronautics and Astronautics

Abstract

This study develops rendezvous maneuver point conditions that are robust to one dimensional errors in state estimation and burn execution. Allowing small deviations in the time of intercept provides a degree of freedom that can be used to compensate for these errors. The direction of allowable burn deviation is developed for errors in state estimation and burn execution. The maneuver points for which the error is aligned with the insensitive direction provide excellent rendezvous initiation points.

The method is applied to sample rendezvous for vehicles in circular and elliptic orbits. Robust maneuver points are selected and the vehicles' relative motion plotted, demonstrating the validity of the maneuver points. Finally, a graphical illustration of the error focusing effect is demonstrated by means of a Monte Carlo simulation.

Thesis Supervisor: Dr. Richard H. Battin
Title: Adjunct Professor of Aeronautics and Astronautics

Technical Supervisor: Peter M. Kachmar
Title: Group Leader, The Charles Stark Draper Laboratory

Technical Supervisor: Stanley W. Shepperd
Title: Staff Engineer, The Charles Stark Draper Laboratory

Acknowledgments

I would like to express my gratitude to all those who have supported me throughout the course of my graduate work at MIT and particularly to those who have had a part in the creation of this thesis.

I thank the people in the Air Force Military Personnel Center and at the Air Force Institute of Technology for this assignment.

I thank John Sweeney and Joan Morrison for keeping a watch on me and on all of the paperwork.

I thank my thesis supervisor, Peter Kachmar, for presenting the problem, and Stan Shepperd, for his help in solving it.

I thank Dr. Battin for his instruction in astrodynamics. His enthusiasm and expertise helped convert me from the aeronautical engineer that I was to the astronautical engineer that I needed to be.

I thank my family and friends for caring.

This thesis was prepared at The Charles Stark Draper Laboratory, Inc., under NASA Contract #NAS9-18426.

Publication of this thesis does not constitute approval by the Draper Laboratory or the sponsoring agency of the findings or conclusions contained herein. It is published for the exchange and stimulation of ideas.

I hereby assign my copyright of this thesis to The Charles Stark Draper Laboratory, Inc., Cambridge, Massachusetts.

<div style="text-align: right;">

_____

Debra Ann Fogle

</div>

Permission is hereby granted by The Charles Stark Draper Laboratory, Inc., to the Massachusetts Institute of Technology to reproduce any or all of this thesis.

Table of Contents

List of Figures

9

10

List of Tables

List of Symbols

Symbol

r	position
v	velocity
h	angular momentum
t	time
f	true anomaly
Θ	central transfer angle
Δ	difference between post-burn and pre-burn, difference between transfer completion and initiation
Φ	transition matrix
e	eccentricity
ε	scale factor
$\delta\theta$	rotation angle
a	semi-major axis
b	semi-minor axis
ϕ	angle between error ellipsoid major axis and defined x axis, angle between existing error and allowable error
γ	elevation angle
i	unit vector

Subscript

C	chaser
T	target
0	initiation of transfer
1	completion of transfer
K	Kepler
L	Lambert
$\perp$	perpendicular component
$\parallel$	parallel component
a	apoapse
p	periapse
req	required for rendezvous
act	actual
est	estimated
T/C	difference between target and chaser
C/T	difference between chaser and target
TOT	sum of initial and final

Superscript

-	pre-burn
+	post-burn
-1	inverse

Acronym

CSI	Coelliptic Sequence Initiation
IMU	Inertial Measurement Unit
LOS	Line-of-Sight
LVLH	Local Vertical, Local Horizontal coordinate system
MC	Correction Maneuver
TI	Transfer Initiation
TPI	Transfer Phase Initiation

Chapter 1

Introduction

Rendezvous of chaser and target vehicles has been and will continue to be an important technological capability required to support space exploration and space utilization programs. This ability to safely and effectively meet up with another object in space is necessary for various types of missions, from transfer of personnel or supplies to rescue, retrieval, repair, inspection, or assembly of orbital units. Rendezvous capability made the Apollo moon landings possible and allows the Space Shuttle to retrieve and repair Earth satellites. It will be required for the build up and resupply of Space Station Freedom and will be essential for the development of Lunar and Martian outposts.

The mission planner must select the best rendezvous scheme under diverse, and possibly conflicting, mission constraints. For example, the planner must trade off fuel expenditure against duration of the rendezvous phase. Throughout rendezvous, the relative range from one craft to the other should be small enough to allow for navigation. The intervals between the various burns must be large enough to permit tracking and to allow preparation for the subsequent maneuver. For safety and control purposes, the closing velocity should not be excessive. The final approach geometry should produce lighting conditions which are favorable to sensor tracking. Furthermore, certain constraints may be imposed on the maneuvers to allow for manual modes of operation if the automatic systems fail.

1.1 Background

Rendezvous technologies developed for the Apollo and Skylab programs involved chaser and target vehicles in near-circular orbits (orbits of very low eccentricity). Both programs employed rendezvous profiles which consisted of similar maneuvers to control the closure phasing and height of the active vehicle (chaser) relative to the passive vehicle (target).

For typical Apollo and Skylab missions (Figure 1.1), the first few maneuvers placed the chaser in a coplanar intermediate phasing, or staging, orbit. This orbit was coelliptic[1] with that of the target at a slightly lower altitude so that the chaser caught up slowly from below and behind. These coelliptic orbits provided minimal altitude variation as the chaser gradually closed on the target.
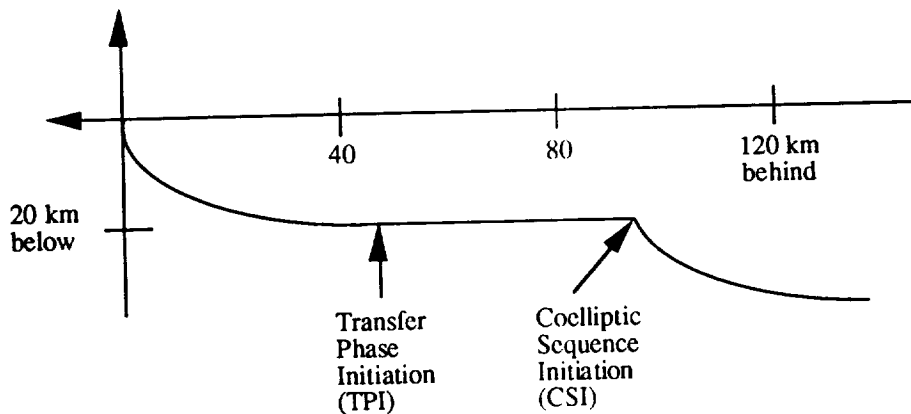
Figure 1.1 Apollo/Skylab Coelliptic Rendezvous Profile

---

[1]The product of the semi-major axis and the eccentricity of the staging orbit is equal to that of the target orbit, and the line of apsides of the staging orbit is coincident with that of the target orbit.

Once the chaser had reached a desired elevation angle of the line-of-sight from the chaser to the target (in the chaser's local vertical frame), the chaser would execute the intercept maneuver and place itself on an intercept trajectory (the transfer phase). Midcourse correction maneuvers were made to maintain the intercept trajectory. The final braking maneuvers were then executed to provide the proper attitude and rate of closure for docking.

This rendezvous strategy allowed for standardization of transfer profiles. Use of the coelliptic phasing orbits resulted in reasonably low, nearly constant closing rates prior to transfer phase initiation (TPI) and standard lighting and approach conditions at completion. This simplified training and mission planning and allowed backup calculation of the burn, independent of the onboard computer. In addition, small burn magnitudes were required, minimizing the effects of a poorly executed maneuver. While the use of phasing orbits requires more fuel and takes longer than a direct transfer, the benefits far outweigh the costs.

The Shuttle rendezvous procedure is somewhat different in that the phasing portion of the profile does not maintain a coelliptic closure with the target, but instead employs an orbit which intercepts the target altitude (Figure 1.2) allowing for "stable" active vehicle standoff conditions if the need arises. Transfer is initiated from this staging orbit. After transfer is initiated (TI), the second correction maneuver (MC2) employs the same elevation angle condition as used in Apollo and Skylab. These maneuvers result in closure rates and relative geometries similar to those in Apollo and Skylab rendezvous.

21
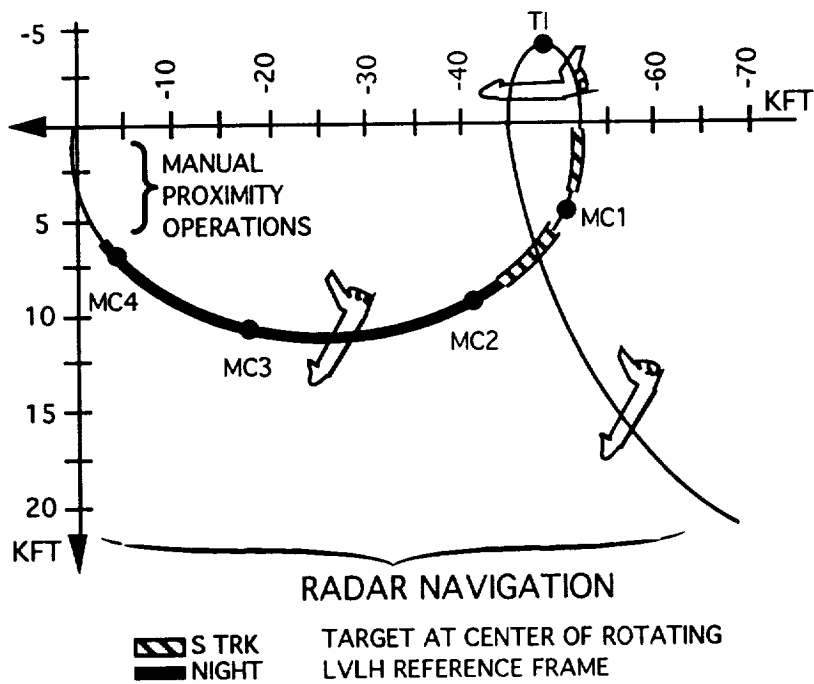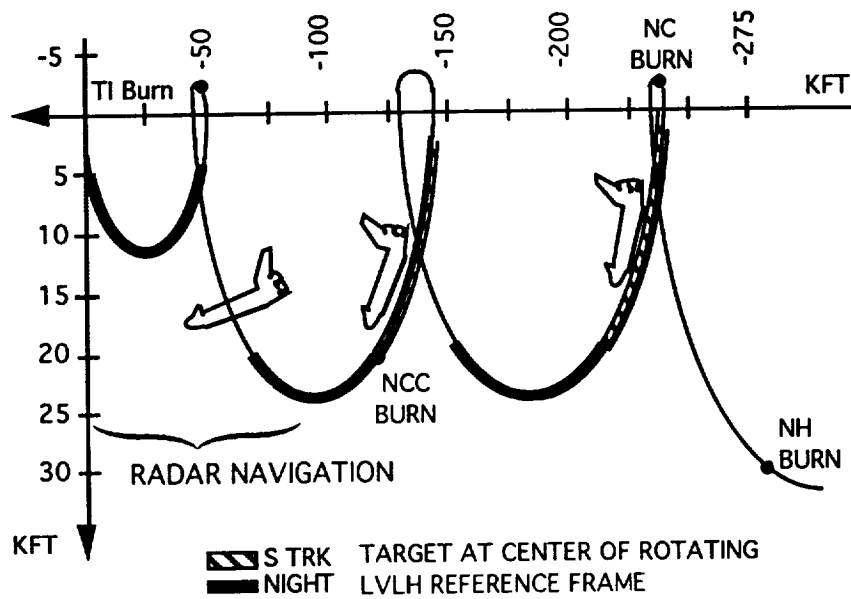
Figure 1.2 Shuttle Rendezvous Profile

While the Apollo and Shuttle rendezvous strategies were developed for targets in near-circular orbits, missions to Mars may require rendezvous with targets in non-circular orbits. Some of the current mission scenarios have created an interest in the development of highly elliptic rendezvous capability. In these scenarios, the heavy interplanetary vehicle is parked in a high-energy, highly elliptic orbit instead of the traditional low-energy circular orbit. Only the small landing craft is taken down to a low circular orbit and/or down to the surface. This approach avoids the fuel penalties associated with taking such a heavy platform down to a low altitude orbit only to have to lift it back up later.

1.2 Error Sources

Most rendezvous studies have focused on fuel minimization with little regard for operational or navigation concerns. With the fuel saved by leaving the heavier platform in orbit, rendezvous studies can now focus on other criteria. Obviously, the result must still be reasonably fuel efficient and cannot be done with a total disregard to fuel usage.

In general, applying an incorrect burn at transfer initiation - whether because of targeting errors due to navigation uncertainties or because of maneuver execution errors - will result in a failed rendezvous. Since the primary goal for rendezvous missions is to bring two vehicles to intercept, the actual time that intercept occurs is of less importance than the fact that it does occur at some point in the trajectory.

Any error in burn estimation or implementation will result in an error in the position of the chaser at the nominal intercept time. Angular measurements supply direct information about line-of-sight (LOS) from the chaser to the target, but only very indirect information about range along that LOS. On the other hand, with range only measurements, the

23

chaser will have very good knowledge of its range to the target and imperfect knowledge of the direction of the LOS. Furthermore, the beginning and ending of a burn can only be controlled to the frequency at which the onboard software is cycled. Also, translation engines have a finite rise and tail off time, further affecting the Δv imparted to the chaser. In addition, control of the burn direction depends on the accuracy of the inertial measurement unit (IMU), which drifts over time, as well as the attitude deadband of the active vehicle. By allowing a small variation in the transfer time of the intercept trajectory, we gain a much-needed degree of freedom that can be used to compensate for selected one-dimensional errors in estimation or execution of the intercept maneuver (TPI in Figure 1.1).

1.3 Overview

This thesis will develop rendezvous maneuver point conditions which provide error tolerance. Targeting of an intercept maneuver is only as accurate as estimate of the relative state between the chaser and the target. Even if the relative state were known exactly (so that the required change in velocity can be calculated exactly), intercept burn execution errors would still limit the ability to rendezvous successfully.

1.3.1 Time as a Degree of Freedom

Given that it is more important for rendezvous to take place at some point along the trajectory than that it occur at a particular time, we can allow the time of intercept to vary in order to ensure that a rendezvous does, in fact, occur. There are two ways to view the use of this degree of freedom to yield insensitivity to errors. We can view the effect of the one-dimensional errors as a velocity error at transfer initiation and search for times when this velocity error is aligned with the one direction of freedom in post-burn

24

velocity. Or we can see the effect of the errors as position errors at intercept and perform the same type of alignment with the relative velocity of the two vehicles at intercept. This thesis will take the first approach. The second approach results in equivalent maneuver point conditions, but in terms of the Kepler transition matrix instead of those of the Lambert transition matrix. These alternate forms are developed in Appendix A. Chapter 2 identifies the freedom in the required burn obtained by allowing small variations in time of intercept.

1.3.2 Execution Error Tolerance

Chapter 3 presents the analytic development of maneuver point conditions which will result in a rendezvous which is insensitive to errors in maneuver execution (i.e., burn magnitude, direction, and ignition time). We will demonstrate the validity of these maneuver point conditions by applying them to rendezvous with targets in both circular and elliptic orbits. We will first place the target in a circular Earth orbit at 350 km with the chaser in a cocircular orbit 20 km below, chosen to be representative of Apollo and Skylab missions.[2] Because of the interest in highly elliptic orbits for missions to Mars, we will then place the target in a highly elliptic Martian orbit with a period approximately equal to one Martian day ($r_p = 500$ km and $r_a = 33000$ km) and the chaser in either a scaled elliptic[3] or coelliptic orbit, (Figure 1.3) each with 20 km decrease in the semi-major axis.

---

[2]These robust maneuver point conditions are also readily applicable to transfer from the more complex staging orbits used by the Shuttle.

[3]The eccentricity of the staging orbit is equal to that of the target orbit, and the line of apsides of the staging orbit is coincident with that of the target orbit.
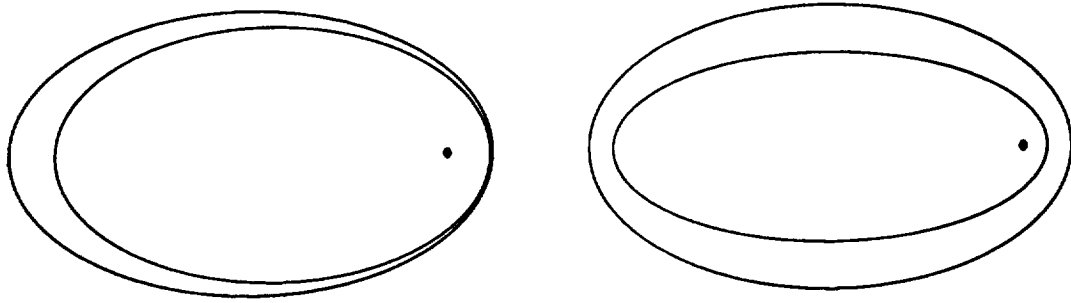
Figure 1.3 Scaled Elliptic and Coelliptic Staging Orbits

1.3.3 Navigation Error Tolerance

In Chapter 4, we will investigate errors in the estimate of the relative state of the chaser. We will then use the freedom in intercept time to develop maneuver point conditions robust to these types of errors. We will perform deterministic flyout from a maneuver point and plot the resulting relative motion as we did in Chapter 3. We will further demonstrate the validity of the maneuver point conditions by generating dispersed states typical of line-of-sight and range measurements respectively, propagating the states to intercept, and observing the focusing effect.[4]

---

[4]The dispersed chaser states converge on the target, although at different times.

Chapter 2

Variation in Time of Intercept

2.1 Derivation of Degree of Freedom

By allowing a small variation in the time of intercept (t_1), we create a degree of freedom that can be used to compensate for any one-dimensional error. Such errors may result from burn execution errors, navigational uncertainties, or some combination of both. In order to make use of this freedom in initial burn, we must first identify it. The velocity that the chaser must achieve at transfer initiation is a function of the transfer time involved ($\Delta t = t_1 - t_0$), the initial position of the chaser ($\underline{r}_C(t_0)$), and final position of the target ($\underline{r}_T(t_1)$).

Figure 2.1 Rendezvous in Inertial Coordinates

This is essentially Lambert's problem:

$$\underline{v}_{req} = \underline{v}_{req}\left(\Delta t, \underline{r}_C(t_0), \underline{r}_T(t_1)\right) \tag{2.1}$$

The required burn is equal to the difference between the required velocity and the pre-burn velocity of the chaser:

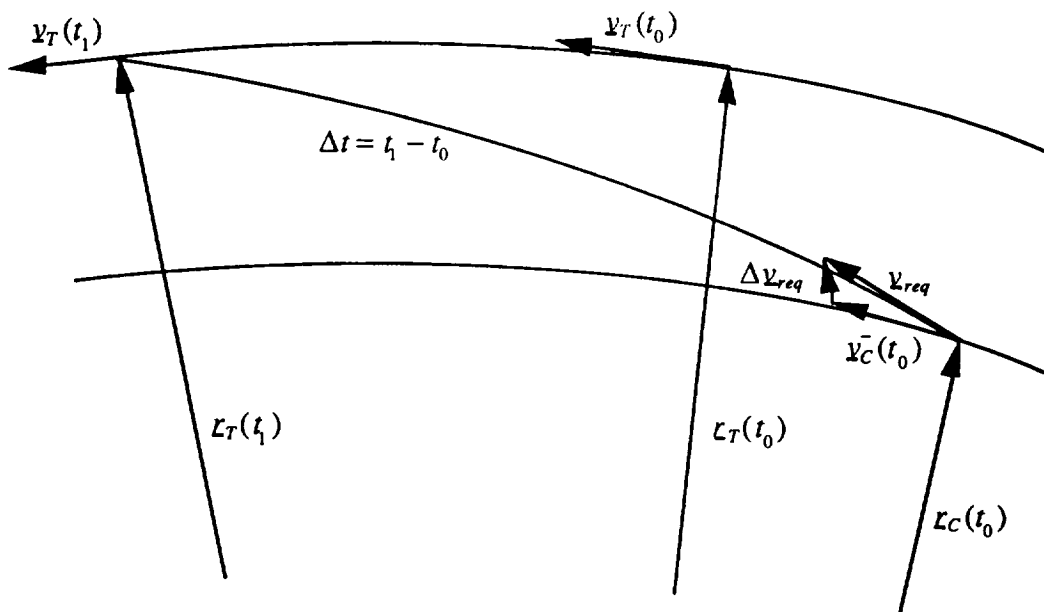$$\Delta \underline{v}_{req} = \underline{v}_{req}\left(\Delta t, \underline{r}_C(t_0), \underline{r}_T(t_1)\right) - \underline{v}_C^-(t_0) \tag{2.2}$$

If we allow small perturbations in any of these variables, the burn required for rendezvous will change. Taking the full differential of Equation 2.1,

$$\delta(\Delta \underline{v}_{req}) = \frac{\partial \underline{v}_{req}}{\partial \Delta t}\delta\Delta t + \frac{\partial \underline{v}_{req}}{\partial \underline{r}_C(t_0)}\delta \underline{r}_C(t_0) + \frac{\partial \underline{v}_{req}}{\partial \underline{r}_T(t_1)}\delta \underline{r}_T(t_1) - \delta \underline{v}_C^-(t_0) \tag{2.3a}$$

Or more compactly,

$$\delta(\Delta \underline{v}_{req}) = \underline{\lambda}_0 \delta\Delta t + L_1 \delta \underline{r}_C(t_0) + L_2 \delta \underline{r}_T(t_1) - \delta \underline{v}_C^-(t_0) \tag{2.3b}$$

where from Lambert's problem

$$\underline{\lambda}_0 \equiv \frac{\partial \underline{v}_{req}}{\partial \Delta t}$$

and L_1 and L_2 are components of the Lambert "transition" (or sensitivity) matrix

$$\begin{bmatrix} \delta \underline{v}_C(t_0) \\ \delta \underline{v}_C(t_1) \end{bmatrix} = \Phi_L \begin{bmatrix} \delta \underline{r}_C(t_0) \\ \delta \underline{r}_T(t_1) \end{bmatrix} = \begin{bmatrix} L_1 & L_2 \\ L_3 & L_4 \end{bmatrix} \begin{bmatrix} \delta \underline{r}_C(t_0) \\ \delta \underline{r}_T(t_1) \end{bmatrix} \tag{2.4}$$

$$L_1 \equiv \frac{\partial \underline{v}_C(t_0)}{\partial \underline{r}_C(t_0)} \qquad L_2 \equiv \frac{\partial \underline{v}_C(t_0)}{\partial \underline{r}_T(t_1)}$$

$$L_3 \equiv \frac{\partial \underline{v}_C(t_1)}{\partial \underline{r}_C(t_0)} \qquad L_4 \equiv \frac{\partial \underline{v}_C(t_1)}{\partial \underline{r}_T(t_1)}$$

Now, if we allow the time of intercept to slip by a small amount, $\delta \Delta t = \delta t_1$. The initial position and velocity of the active vehicle do not change, $\delta \underline{r}_C(t_0) = \delta \underline{v}_C^-(t_0) = \underline{0}$, but final position of the passive vehicle does:

$$\delta \underline{r}_T(t_1) = \underline{v}_T(t_1)\delta t_1 \tag{2.5}$$

The change in the required burn caused by this small time slip is then

$$\delta(\Delta \underline{v}_{req}) = \left[\underline{\lambda}_0 + L_2 \underline{v}_T(t_1) \right] \delta t_1 \tag{2.6a}$$

The first term on the right hand side of this equation is the change in required burn due to a change in intercept time for rendezvous with a fixed point in space. The second term is the change in required burn caused by the movement of the target. Together these effects determine the direction in which the initial post-burn velocity is free to vary.

For convenience, we will define

$$\underline{w}_{t_1} \equiv \underline{\lambda}_0 + L_2 \underline{v}_T(t_1)$$

so that

$$\delta(\Delta \underline{v}_{req}) = \underline{w}_{t_1} \delta t_1 \tag{2.6b}$$

29

Thus, small burn errors which are parallel to $\underline{w}_{t_1}$ result in small final position errors which are parallel to the relative velocity vector at rendezvous, and these errors are absorbed by small variations in transfer time. Small errors in initial post-burn velocity which are perpendicular to $\underline{w}_{t_1}$ result in small final position errors which are perpendicular to the relative velocity vector and therefore result in pure miss distance.

2.2 Linearity Restrictions

The derivation includes assumptions of linearity which place restrictions on the application of this freedom. First, we assume that the variation in the transfer time is small,

$$\frac{\delta \Delta t}{\Delta t} << 1$$

and that the change in the position of the target is small

$$\frac{|\delta \underline{r}_T(t_1)|}{|\underline{r}_T(t_1)|} << 1$$

We also assume that the motion of the target at the intercept point is linear. This assumption of linear motion at intercept is often the most restrictive. The length of time for which this is true may be quite small, particularly near periapse. When we use this degree of freedom to absorb errors, we will have to monitor changes in intercept time to ensure that all of these assumptions hold true.

30

Chapter 3

Execution Error Tolerance

Any error in implementation of the burn will result in an error in the position of the chaser at the nominal intercept time. We will examine three types of burn error: magnitude error, in-plane directional error, and ignition time error. The burn can be expressed as $\Delta \underline{v}_C(t_0) = \underline{v}_C^+(t_0) - \underline{v}_C^-(t_0)$. When the burn is executed exactly, $\underline{v}_C^+(t_0) = \underline{v}_{req}$ and $\Delta \underline{v}_C(t_0) = \Delta \underline{v}_{req}$.

As Figure 3.1 shows, an error in burn magnitude is parallel to $\Delta \underline{v}_{req}$, while a small error in burn direction is perpendicular to $\Delta \underline{v}_{req}$. These errors are the two in-plane components of executing the wrong burn at the right time. The conditions that result in a rendezvous which is robust to small errors in magnitude or direction are developed together in Section 3.1. The condition for robustness to an ignition time error (executing the right burn at the wrong time) is developed in Section 3.2.

Burn Magnitude Error

$\delta(\Delta \underline{v}_C(t_0))_{\shortparallel} = \varepsilon(\Delta \underline{v}_{req})$

Burn Direction Error

$\delta(\Delta \underline{v}_C(t_0))_{\perp} = (\Delta \underline{v}_{req} \times i_h)\delta\theta$
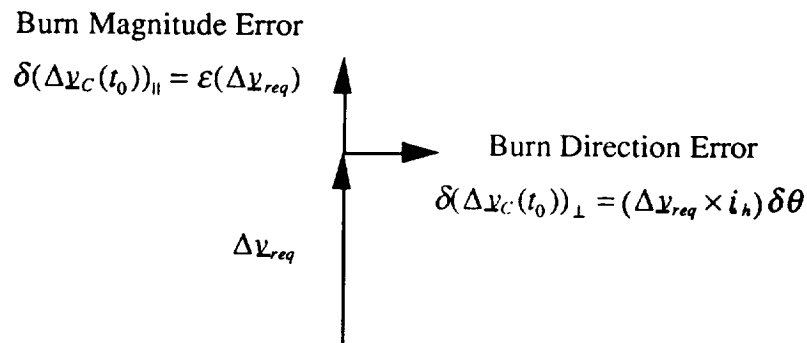
$\Delta \underline{v}_{req}$

Figure 3.1 Burn Magnitude and Direction Errors

31

3.1 Magnitude and Direction Errors

Consider the case in which the burn is applied at the correct time but with an error in either the magnitude or the direction. Since there is no deviation in initial position or velocity of the chaser ($\delta \underline{r}_C(t_0) = \delta \underline{v}_C^-(t_0) = \underline{0}$) and the final position of the target is unchanged, the required burn is unchanged.

In order for rendezvous to occur, the error in the burn must be equal to the acceptable deviation in the burn associated with the variation in intercept time:

$$\delta(\Delta \underline{v}) = \delta(\Delta \underline{v}_{req}) = \underline{w}_{t_1} \delta t_1 \tag{3.1}$$

In the case of a burn magnitude error, $\delta(\Delta \underline{v})_\parallel$,

$$\delta(\Delta \underline{v})_\parallel \equiv \varepsilon \Delta \underline{v}_{req} = \underline{w}_{t_1} \delta t_1 \tag{3.2}$$

For this to be true, the two vectors must be parallel or anti-parallel:

$$\Delta \underline{v}_{req} \times \underline{w}_{t_1} = \underline{0} \tag{3.3}$$

Thus, Equation 3.3 is the maneuver point condition defining insensitivity to burn magnitude errors. The corresponding intercept time variation is

$$\delta t_1 = \varepsilon \frac{\Delta \underline{v}_{req} \cdot \underline{w}_{t_1}}{\underline{w}_{t_1} \cdot \underline{w}_{t_1}} = \pm \varepsilon \frac{\left| \Delta \underline{v}_{req} \right|}{\left| \underline{w}_{t_1} \right|} \tag{3.4}$$

In the case of an error in burn direction, $\delta(\Delta \underline{v})_\perp$,

32

$$\delta(\Delta \underline{v})_{\perp} \equiv \left(\Delta \underline{v}_{req} \times \underline{i}_{h} \right) \delta \theta = \underline{w}_{t_{1}} \delta t_{1}$$
(3.5)

where $\underline{i}_{h}$ is a unit angular momentum vector (perpendicular to the orbital plane). For this to occur, the burn direction error must again be parallel or anti-parallel to the acceptable deviation in the burn

$$\delta(\Delta \underline{v})_{\perp} \times \underline{w}_{t_{1}} = \underline{0}$$

$$\Delta \underline{v}_{req} \cdot \underline{w}_{t_{1}} = 0$$
(3.6)

Equation 3.6 is the robust maneuver point condition for burn direction errors. The resulting variation in the time of intercept is

$$\delta t_{1} = \frac{\left(\Delta \underline{v}_{req} \times \underline{i}_{h} \right) \cdot \underline{w}_{t_{1}}}{\underline{w}_{t_{1}} \cdot \underline{w}_{t_{1}}} \delta \theta = \pm \frac{\left| \Delta \underline{v}_{req} \right|}{\left| \underline{w}_{t_{1}} \right|} \delta \theta$$
(3.7)

These two maneuver point conditions are complementary and span the space of in-plane burn execution errors. Clearly, these conditions cannot occur simultaneously. A maneuver point condition can be chosen which is insensitive to a burn magnitude error or one which is insensitive to a burn direction error, but not one which is insensitive to both at the same time. However, if a specific combination of magnitude and direction error (an error confined to one dimension) is expected, we can develop a maneuver point condition which is robust to that error instead.

3.2 Ignition Time Error

If we delay execution of the burn by some small amount of time, δt_0, the chaser's initial state, both position and pre-burn velocity, will change slightly:

$$\delta \underline{r}_C(t_0) = \underline{v}_C^-(t_0)\delta t_0$$
$$\delta \underline{v}_C^-(t_0) = \underline{g}_C(t_0)\delta t_0 = -\frac{\mu}{\left|\underline{r}_C(t_0)\right|^3}\underline{r}_C(t_0)\delta t_0 \tag{3.8}$$

Because of this delay, the chaser has less time to arrive at the nominal intercept point:

$$\delta \Delta t = -\delta t_0 \tag{3.9}$$

Substituting Equations 3.8 and 3.9 into Equation 2.3, the deviation in the required burn is

$$\delta(\Delta \underline{v}_{req}) = \left[-\underline{\lambda}_0 + L_1 \underline{v}_C^-(t_0) - \underline{g}_C(t_0)\right]\delta t_0 \tag{3.10a}$$

The first term on the right hand side of this equation is the change in required burn with a change in time of execution for rendezvous from a fixed state in space. The next two terms are the change in required burn caused by the change in the initial state of the chaser. Together these effects determine the direction in which the initial required burn varies.

For convenience, define

$$\underline{w}_{t_0} \equiv -\underline{\lambda}_0 + L_1 \underline{v}_C^-(t_0) - \underline{g}_C(t_0)$$

so that

$$\delta(\Delta \underline{v}_{req}) = \underline{w}_{t_0} \delta t_0 \qquad\qquad (3.10\mathrm{b})$$

In order for rendezvous to occur, this deviation in required burn combined with the deviation in required burn associated with a deviation in time of intercept must be zero.

$$\delta(\Delta \underline{v}_{req}) = \underline{w}_{t_1} \delta t_1 + \underline{w}_{t_0} \delta t_0 = \underline{0} \qquad\qquad (3.11)$$

Equation 3.12 is the maneuver point condition which provides insensitivity to ignition time errors

$$\underline{w}_{t_0} \times \underline{w}_{t_1} = \underline{0} \qquad\qquad (3.12)$$

The corresponding variation in time of intercept is

$$\delta t_1 = -\frac{\underline{w}_{t_0} \cdot \underline{w}_{t_1}}{\underline{w}_{t_1} \cdot \underline{w}_{t_1}} \delta t_0 = \pm \frac{\left| \underline{w}_{t_0} \right|}{\left| \underline{w}_{t_1} \right|} \delta t_0 \qquad\qquad (3.13)$$

A delay (executing the right burn at the wrong time) results in a burn error which is generally some combination of error in magnitude and direction. In special cases, this maneuver point condition may occur simultaneously with one or the other of the previously developed conditions. In other words, we may be able to choose a maneuver point which is robust to both burn magnitude errors and burn ignition time errors or one which tolerates both burn direction errors and burn ignition time errors.

35

3.3 Application of Burn Error Tolerance Conditions to Circular Orbits

With knowledge of the target's orbit and of the chaser's orbit, the various possible transfer alternatives can be searched for those which result in a maneuver point which meets the desired condition. If such maneuver points exist, they can be used to achieve tolerance to whichever type of error is of most concern.

For a given circular orbit pair, a nominal rendezvous is completely defined by the relative true anomaly of the target ($f_{T/C}(t_0) = f_T(t_0) - f_C(t_0)$) and the central transfer angle (Θ).
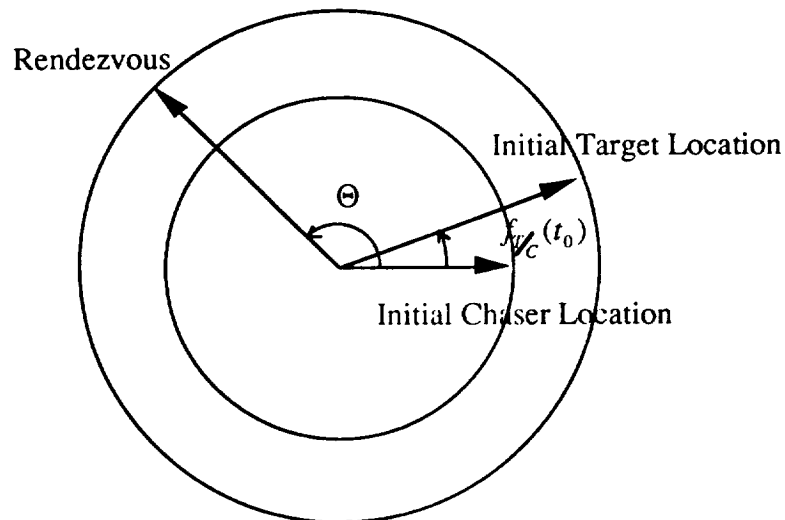
Figure 3.2 True Anomaly and Central Transfer Angle

For each choice of Θ, we will vary $f_{T/C}(t_0)$[1] and plot the angle ϕ (Figure 3.3) between the required burn and the change in the required burn caused by the variation in intercept time (Figure 3.4).

---

[1] $f_{T/C}(t_0)$ must be small to keep fuel consumption reasonable.

36
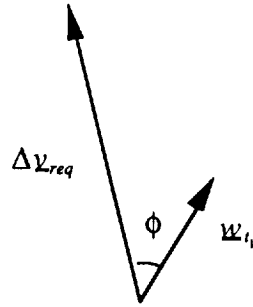
Figure 3.3 Angle Between Required Burn and Change in Required Burn Insensitivity
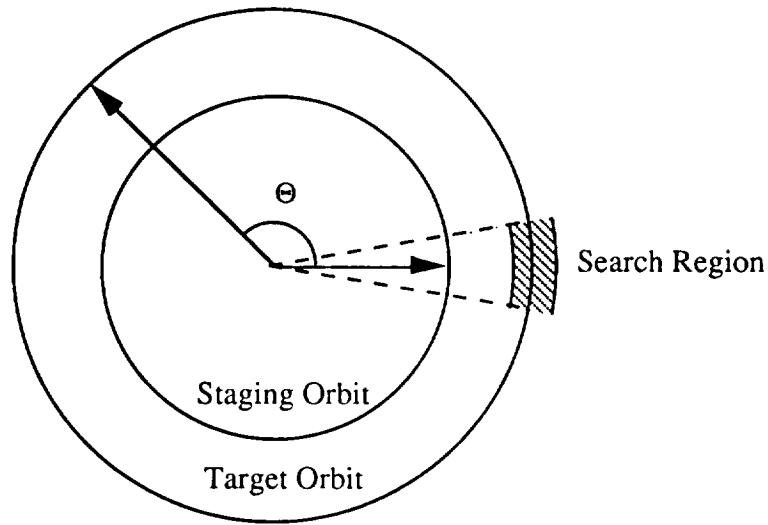   Direction

Figure 3.4 Search Region

When $\phi = n\pi$, the condition for burn magnitude error tolerance (Equation 3.3) is satisfied. Figure 3.5 shows ϕ in a search region of $f_{T/c}(t_0) = \pm 1°$ for three sample central transfer angles. Each crossing of $n\pi$ indicates a choice of maneuver point which is robust to burn magnitude error. Figure 3.6a shows the set of all such points for transfer angles in the range of 45° to 180°. There are two robust maneuver points for each transfer angle.

When $\phi = \dfrac{(2n+1)}{2}\pi$, the condition for burn direction error tolerance (Equation 3.6) is satisfied. Unfortunately, there are no maneuver points that provide insensitivity to burn
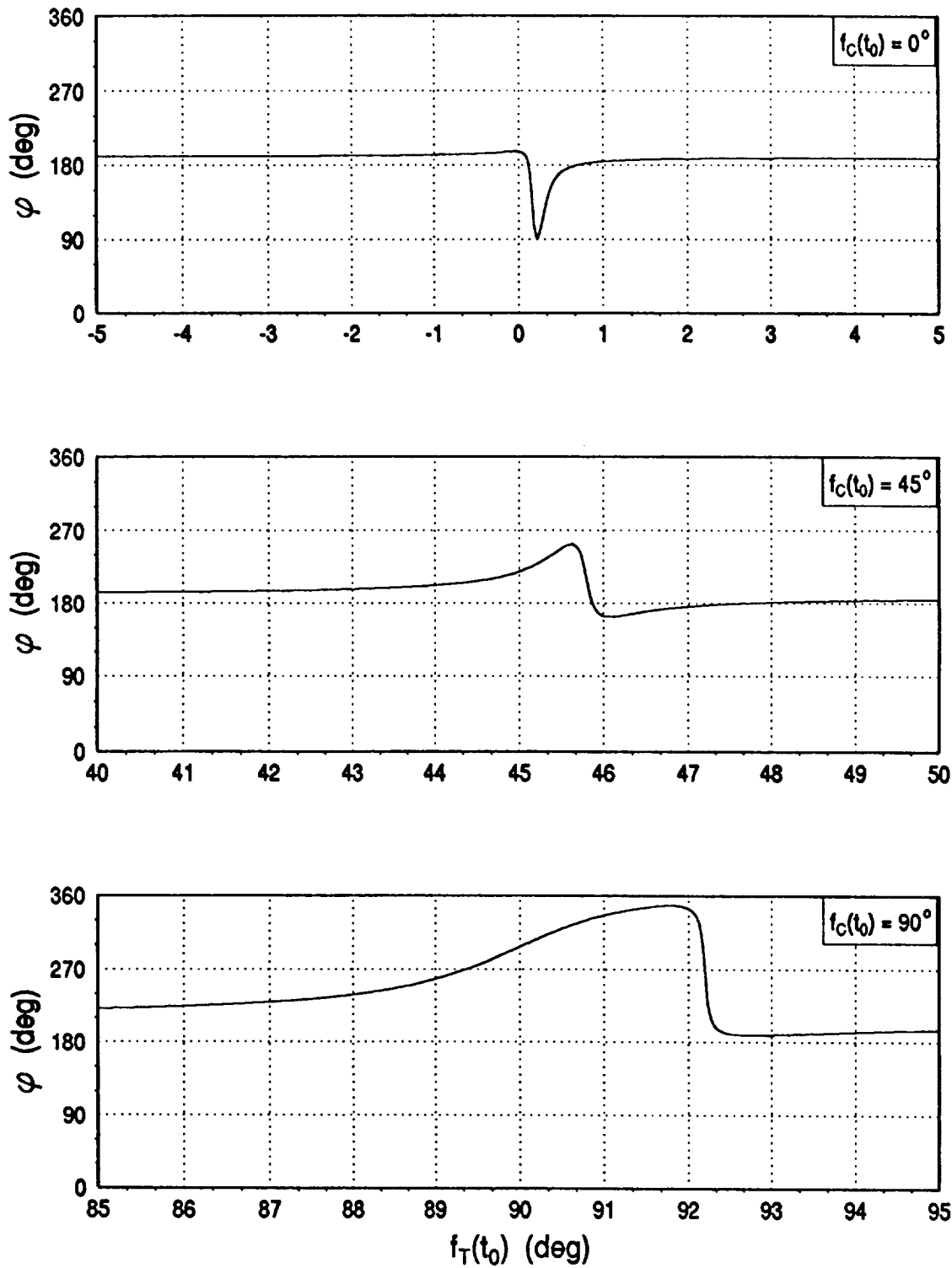
Figure 3.5 Variation in φ -- Burn Magnitude and Direction Errors
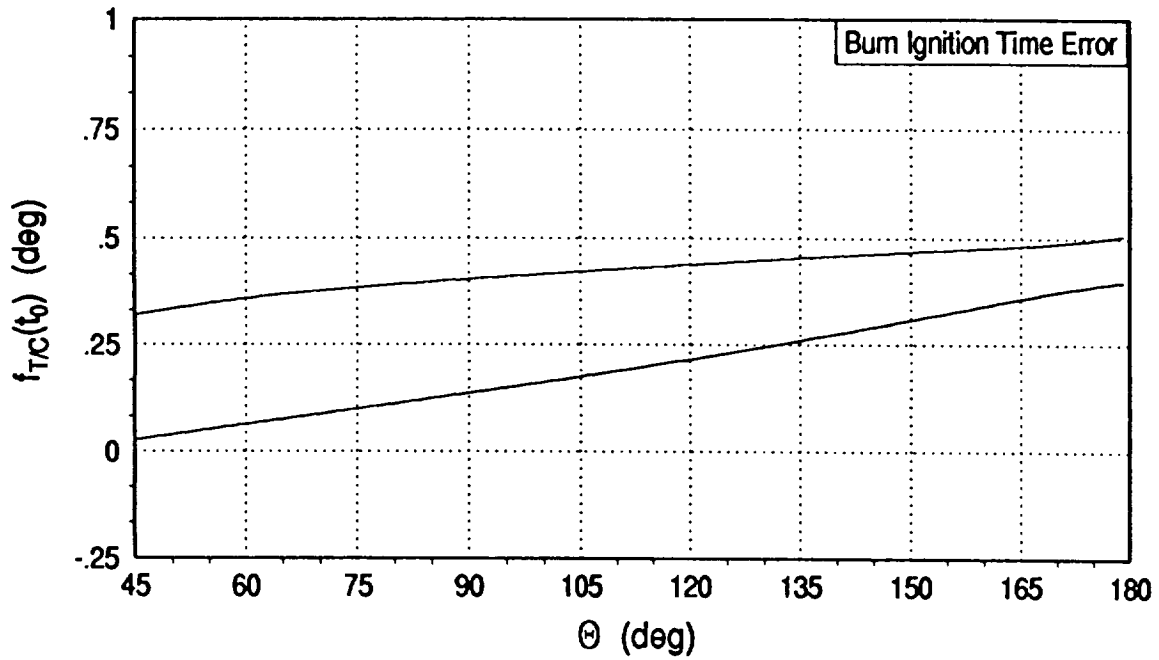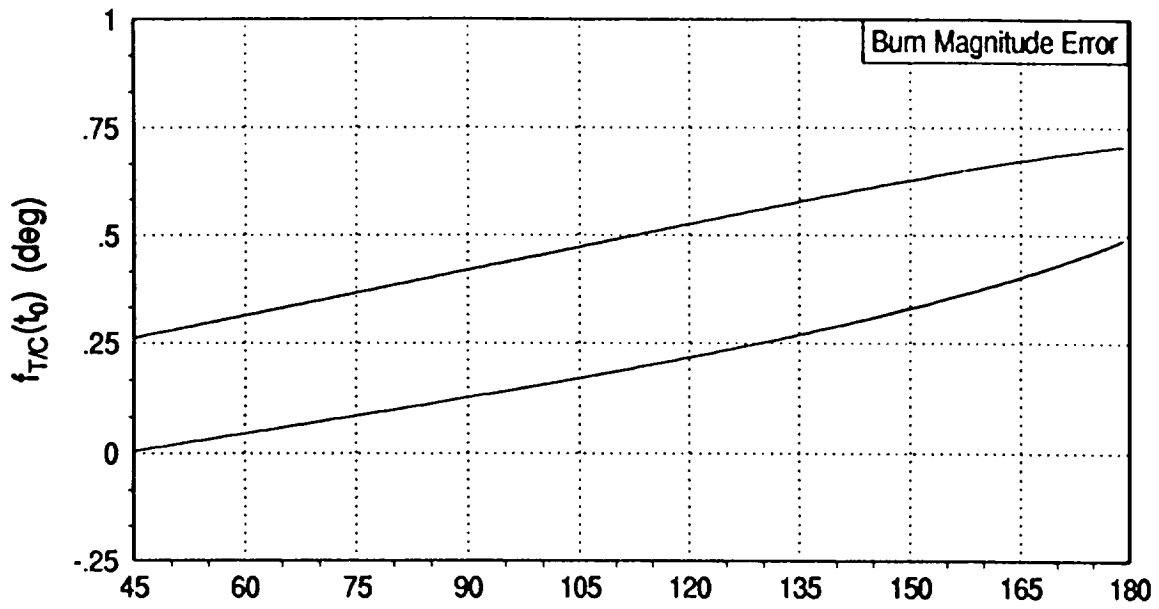
38

Figure 3.6 a&b Burn Execution Error Tolerant Maneuver Points for Cocircular Staging

Orbit

direction error (no $\frac{(2n+1)}{2}\pi$ crossings) for the circular orbit case studied. This means that there are no points at which a burn direction error is perfectly aligned with the allowable deviation in burn. There are regions, however, where these vectors are near to alignment. The component of the direction error along $\underline{w}_{t_1}$ causes a slip in intercept time. The component which is perpendicular to $\underline{w}_{t_1}$ causes a miss distance at intercept. If we minimize this perpendicular component (by choosing maneuver points where the vectors are nearly aligned), we will minimize the miss distance.

For ignition time errors, we examine the angle ϕ between the change in required burn caused by a delay in burn execution and the change in required burn corresponding to a delay in intercept. (Figure 3.7).
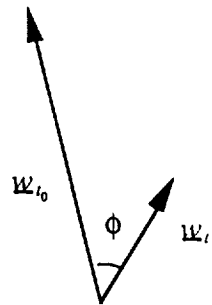

Figure 3.7 Angle Between Change in Required Burn Caused by Execution Time Slip and That Corresponding to an Intercept Time Slip

When $\phi = n\pi$, the condition for tolerance of ignition time errors (Equation 3.12) is satisfied. Figure 3.6b shows the set of all such points for transfer angles in the range of 45° to 180°. There are two robust maneuver points for each initial chaser position throughout the range of transfer angles examined.

Figure 3.8 shows the intercept time slips required to compensate for each type of burn execution error. As expected, an increase in applied burn magnitude will cause the chaser
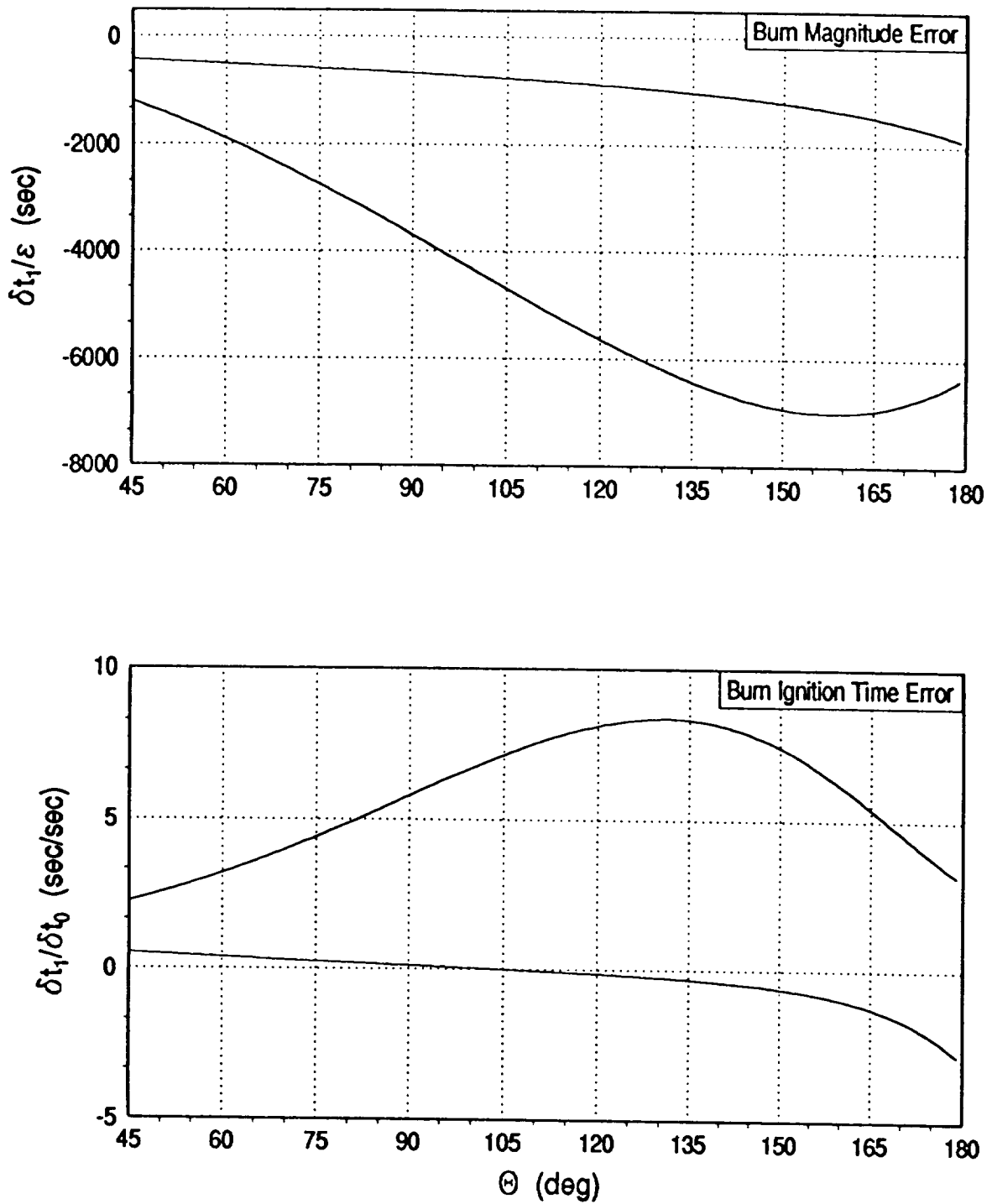
Figure 3.8 Deviation in Transfer Time for Cocircular Staging Orbit

to arrive at intercept sooner (the vectors are anti-parallel: ϕ is an odd multiple of π), and, in general, a delay in the burn will cause a delay in the intercept.

When using near-solution points to compensate for burn direction errors, the intercept time slip is

$$\delta t_1 = \frac{\delta(\Delta \underline{v})_\perp \cdot \underline{w}_{t_1}}{\underline{w}_{t_1} \cdot \underline{w}_{t_1}} \qquad (3.14)$$

3.4 Application of Burn Error Tolerance Conditions to Highly Elliptic Orbits

For highly elliptic orbits, we must choose $f_C(t_0)$, $f_{T/_C}(t_0)$, and Θ to specify a nominal rendezvous.
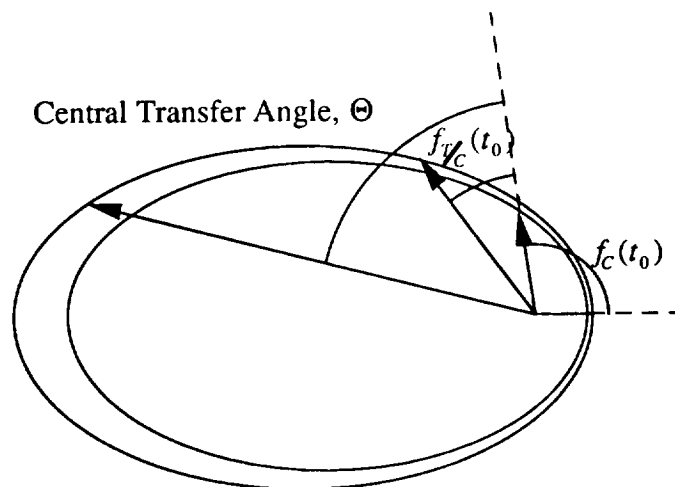
Figure 3.9 True Anomaly and Central Transfer Angle for Elliptic Orbits

We will choose $f_C(t_0)$, and Θ and examine ϕ for a range of $f_{T/_C}(t_0)$ (Figure 3.10). For elliptic orbits, each choice of $f_C(t_0)$ gives us a different solution, so we will fix Θ

(Θ=135°) and examine the entire range of initial chaser positions.[2] Figure 3.11 shows ϕ in a search region of $f_{T/c}(t_0) = \pm 5°$ for three initial chaser locations.
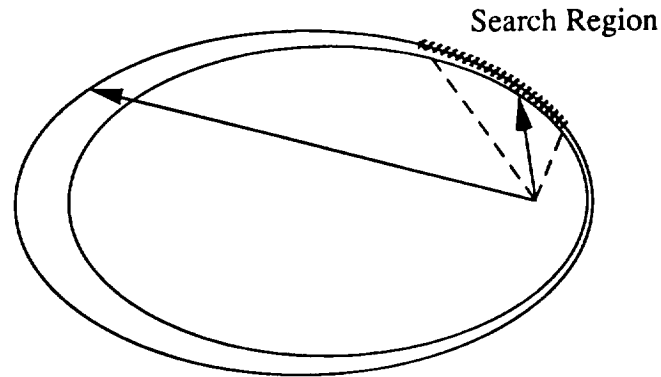

Figure 3.10 Search Region for Elliptic Orbits

Figure 3.12 a,b,&c show maneuver point conditions for transfer from the scaled elliptic staging orbit. Note that in addition to burn magnitude insensitivity points, direction error insensitivity points exist for this scaled elliptic case. Unlike the other regions, for the set of magnitude solutions that are enclosed by direction error solutions (near $f_C(t_0) = 120°$), ϕ is an even multiple of π and an increase in the magnitude of the burn actually results in a delay in intercept. Figure 3.13 a,b,&c show the associated rendezvous time slips. The upper curve in Figure 3.12b causes extremely large time slip errors (Figure 3.13b), violating the linearity assumptions ($\dfrac{\delta(\Delta t)}{\Delta t} \ll 1$). These maneuver points should be avoided. Figures 3.14 and 3.15 do the same for transfer from the coelliptic staging orbit.

Figure 3.16 describes the target-centered curvilinear coordinate system that will be used in the relative motion plots.

―――――――――――

[2]For alternate solution sets, see Appendix C.

43

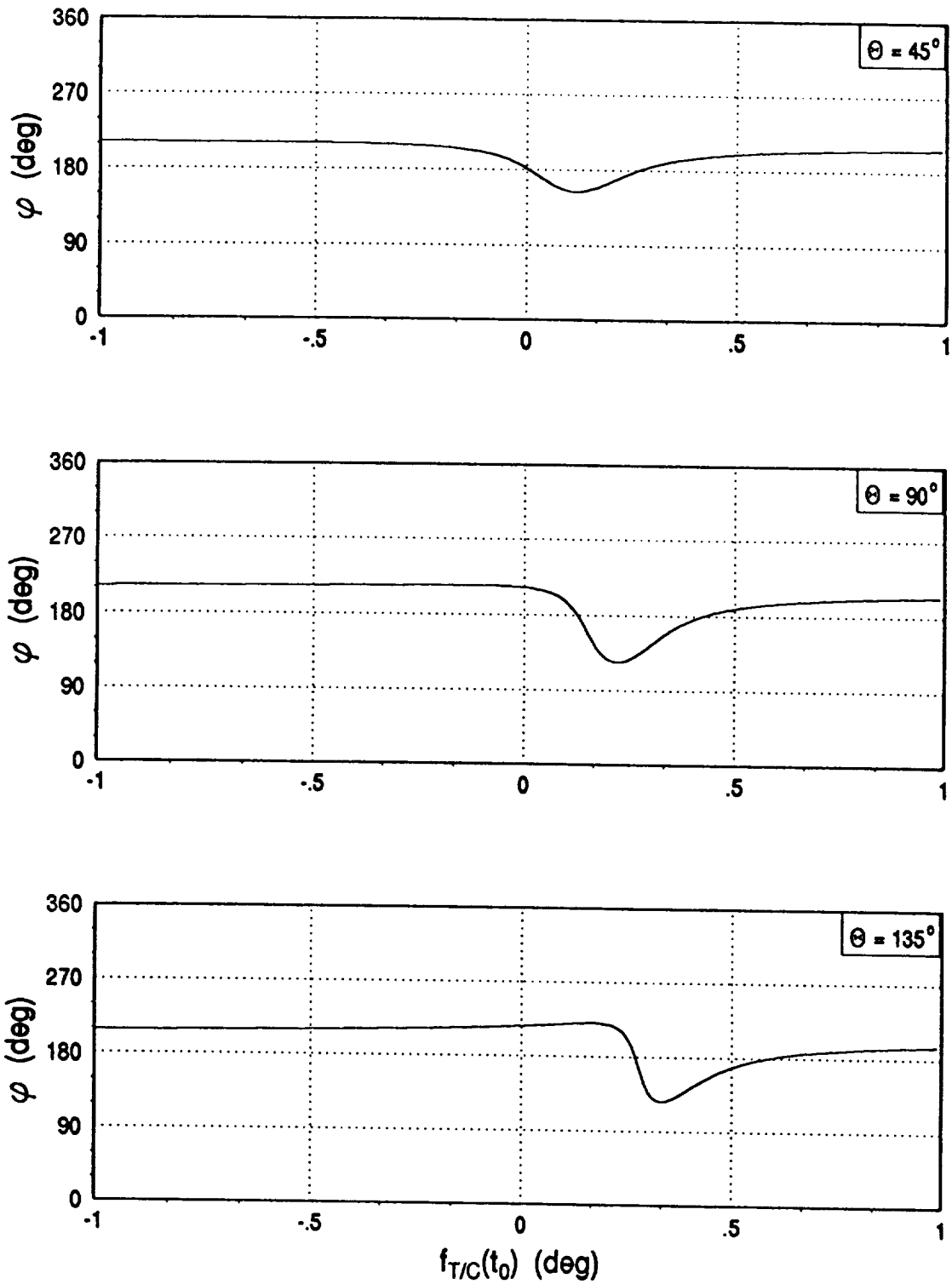Figure 3.11 Variation in φ --Burn Magnitude and Direction Error, Scaled Elliptic Staging
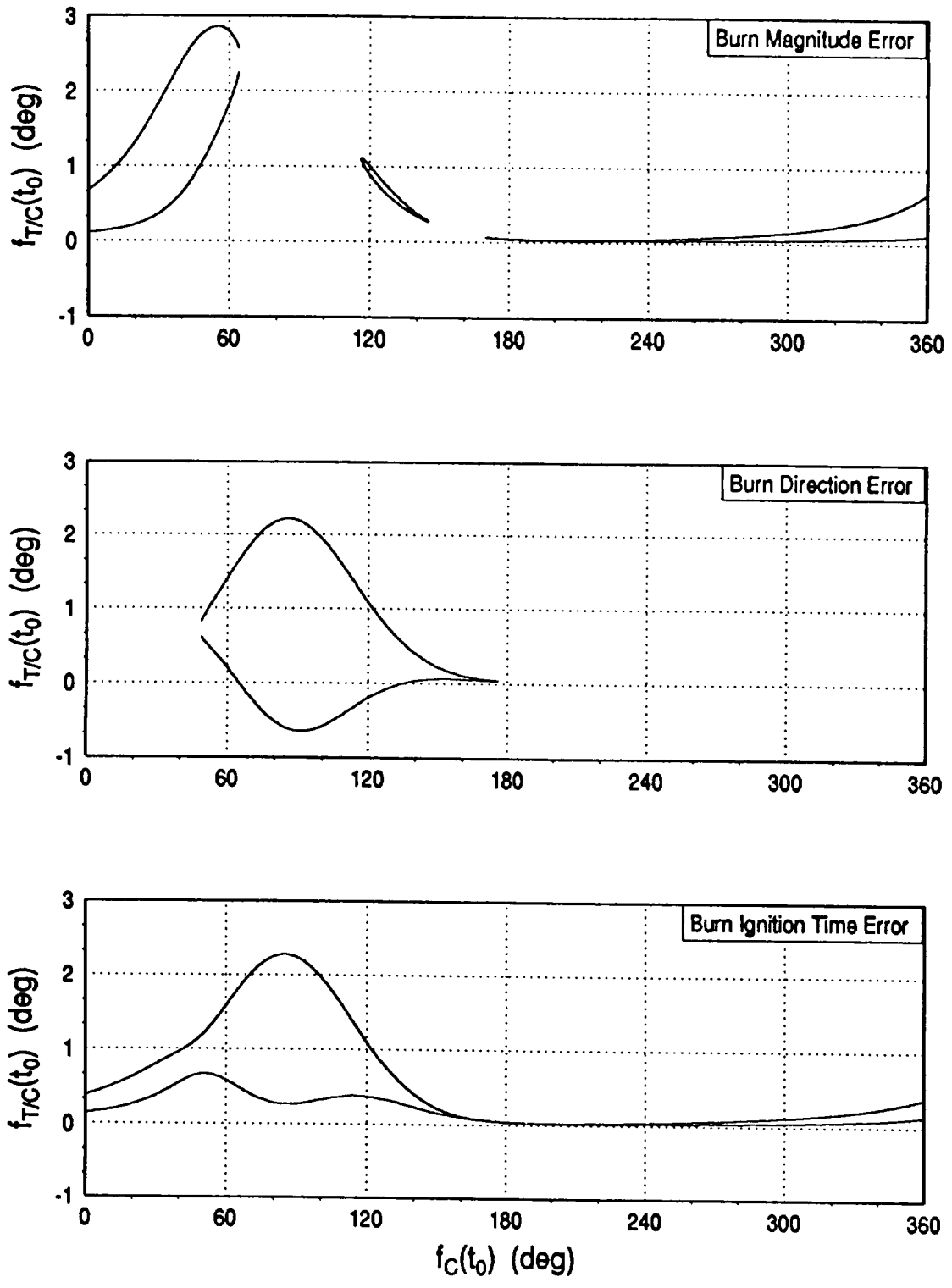
Orbit

Figure 3.12 Burn Execution Error Tolerant Maneuver Points for Scaled Elliptic Staging
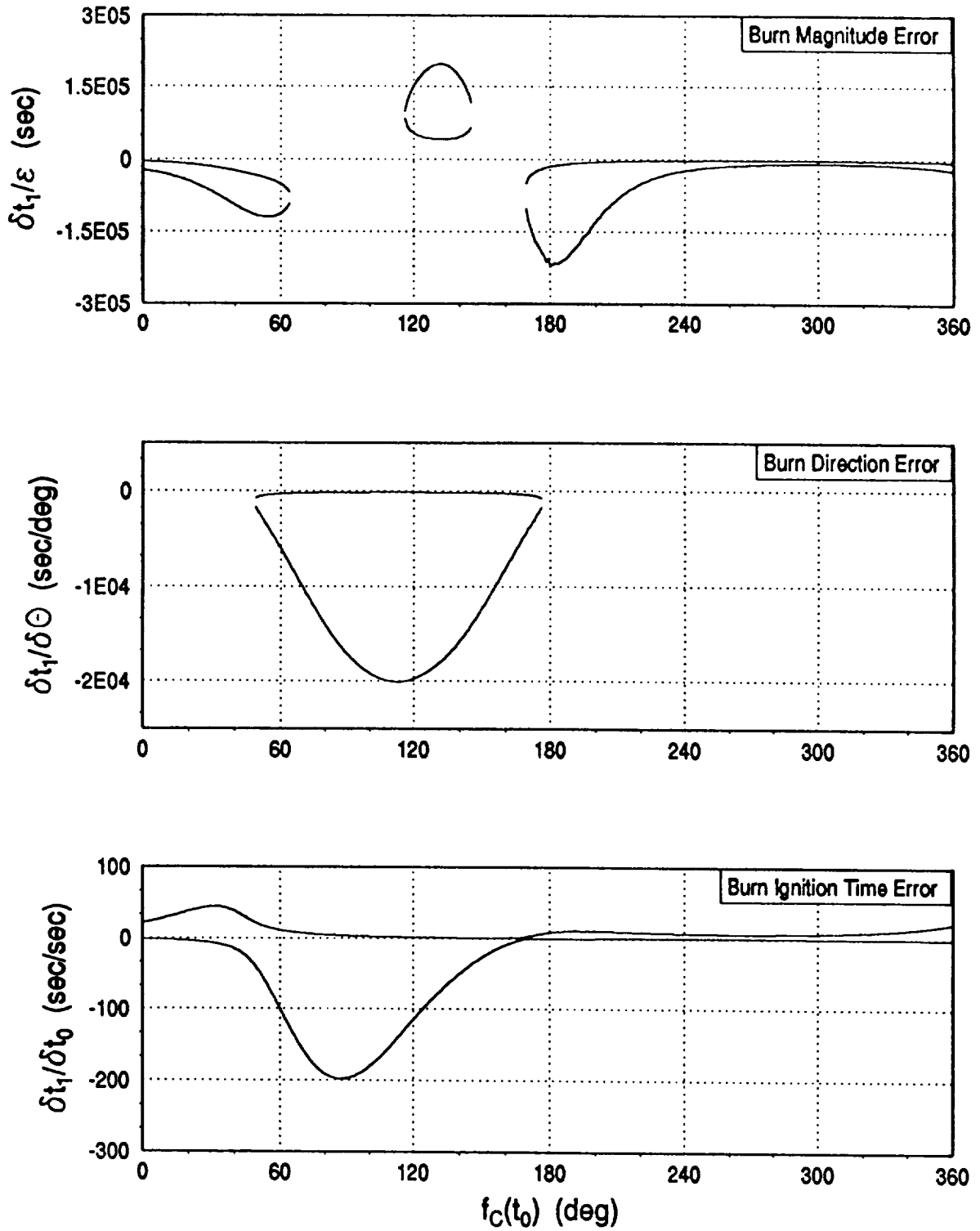
Orbit and 135° Central Transfer Angle

45

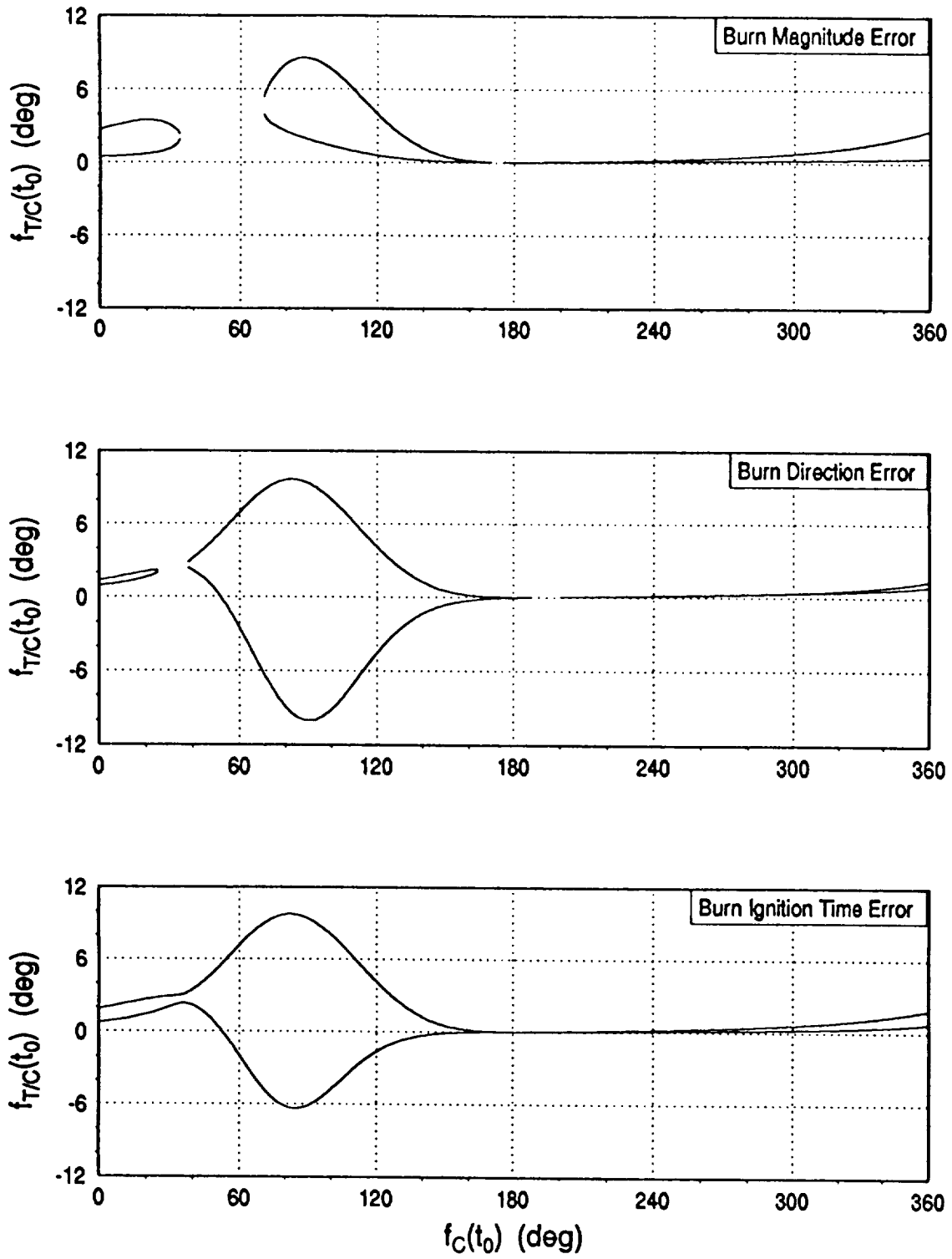Figure 3.13 Corresponding Deviation in Transfer Time -- Scaled Elliptic Staging Orbit

Figure 3.14 Burn Execution Error Tolerant Maneuver Points for Coelliptic Staging Orbit and 135° Central Transfer Angle
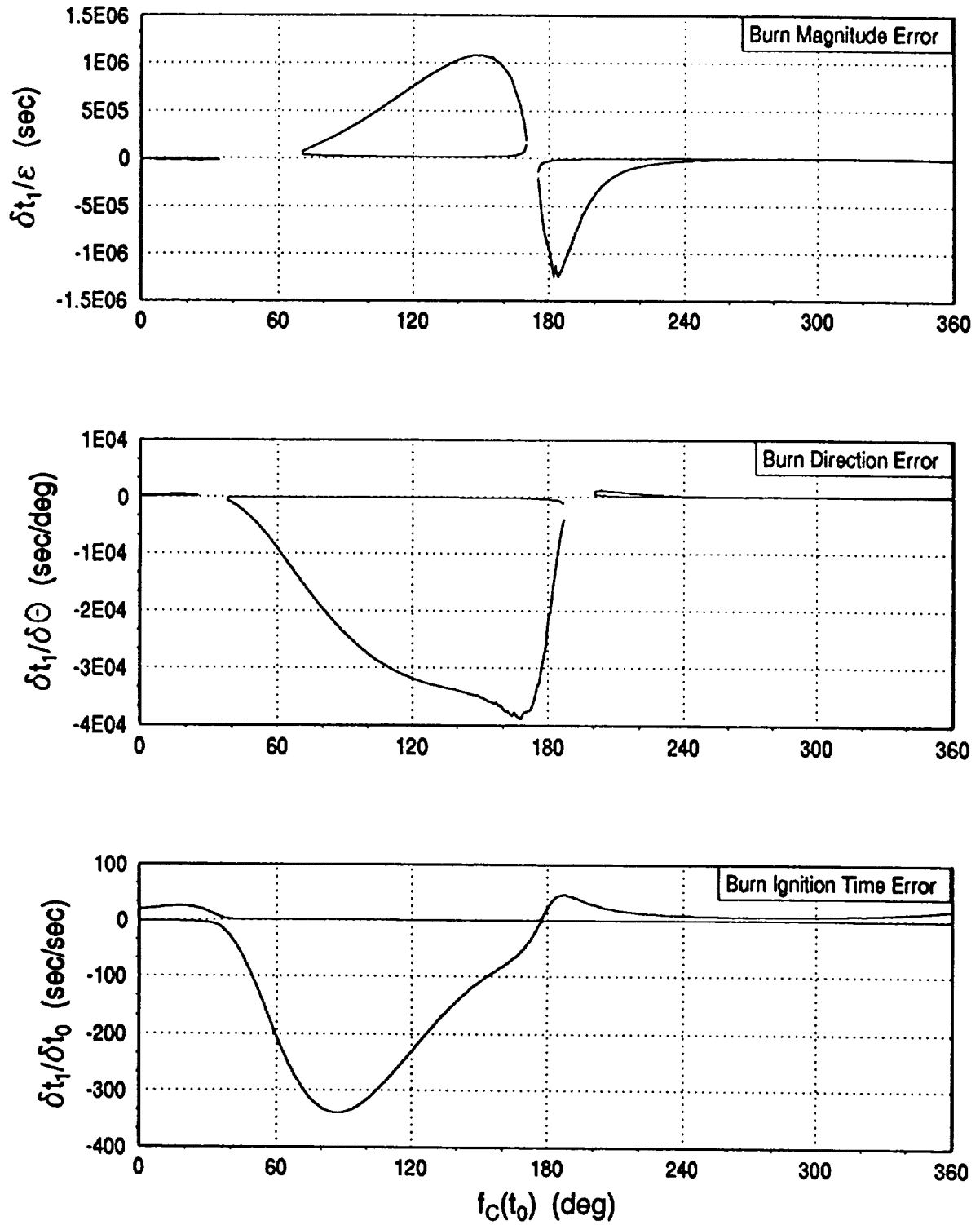
47

Figure 3.15 Corresponding Deviation in Transfer Time -- Coelliptic Staging Orbit
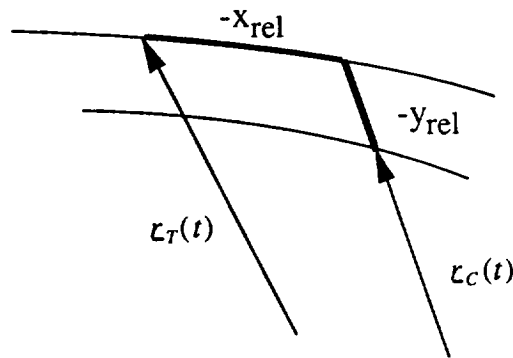
Figure 3.16 Curvilinear Coordinate System

Figure 3.17 shows the relative motion plots for transfer from a burn magnitude error insensitivity point ($f_C(t_0)$=45° and $f_{T_{/C}}(t_0)$=+2.6379° from Figure 3.12a) for each of the three types of burn execution error. Note that in the case of the burn magnitude error, the three dispersed trajectories focus at the target (although at different times). The other two types of errors result in large miss distances. Figure 3.18 repeats this for a burn direction error insensitivity point ($f_C(t_0)$=90° and $f_{T_{/C}}(t_0)$=-0.6416° from Figure 3.12b), and Figure 3.19 for a burn ignition time error insensitivity point ($f_C(t_0)$=90° and $f_{T_{/C}}(t_0)$=+0.2738° from Figure 3.12c). Relatively large errors are used in all three cases so that the effects will be visible.
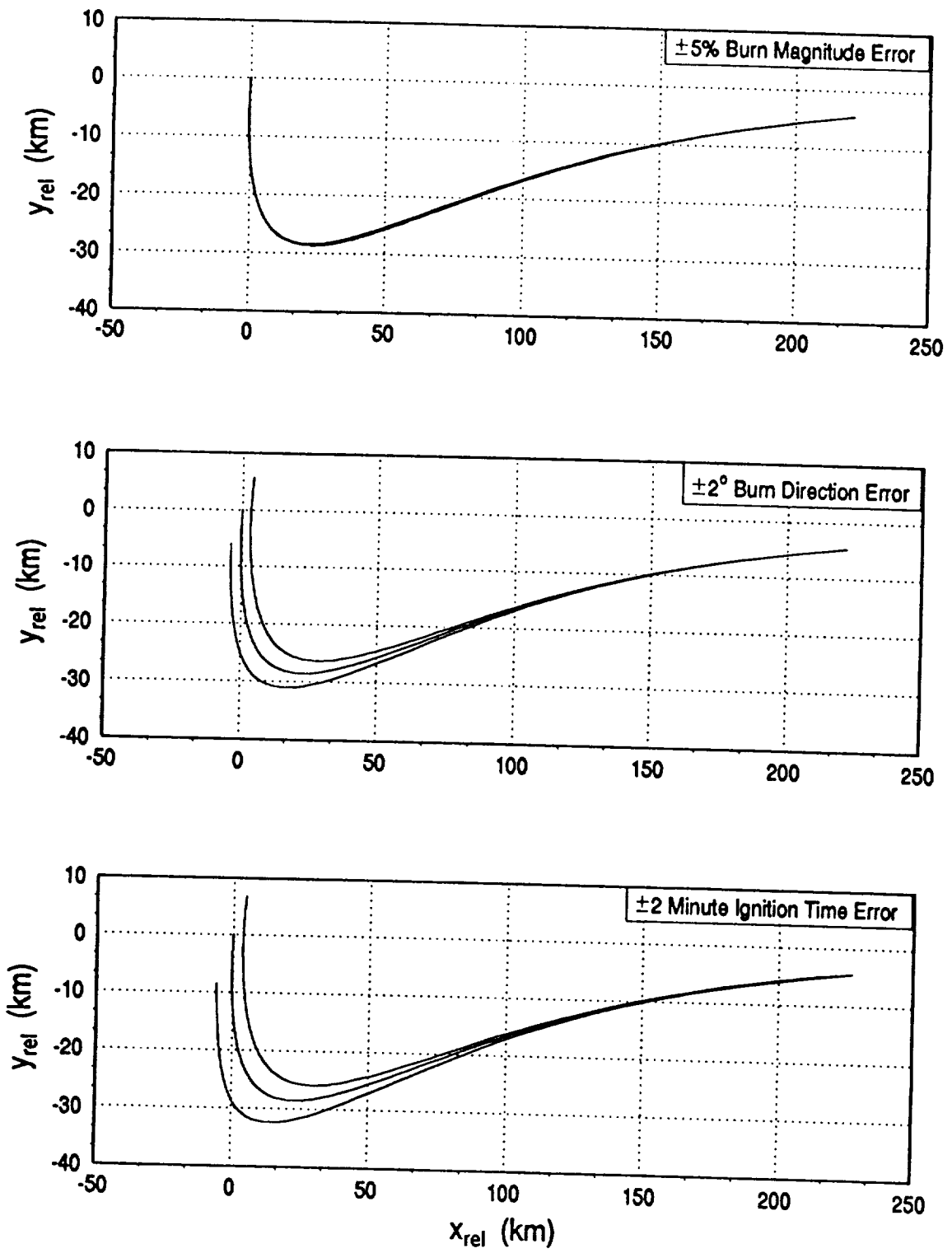
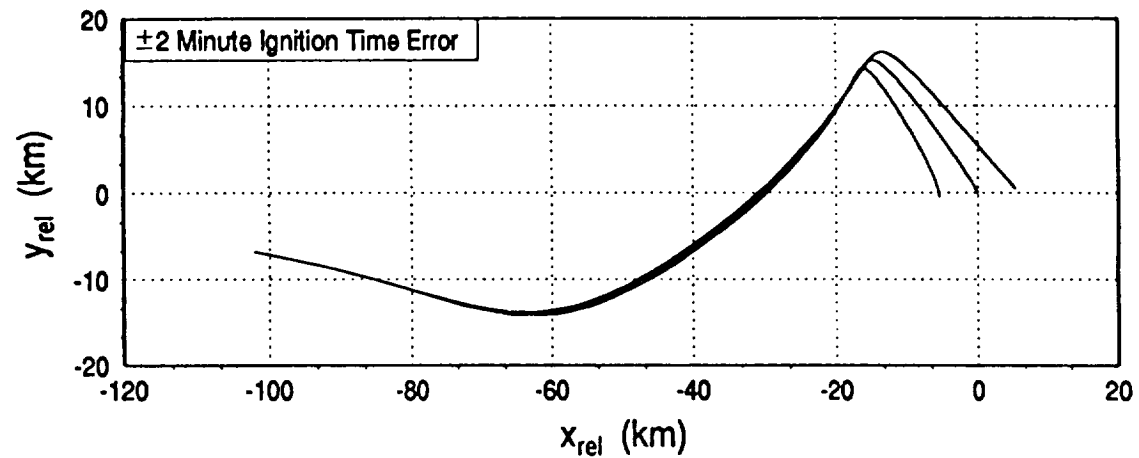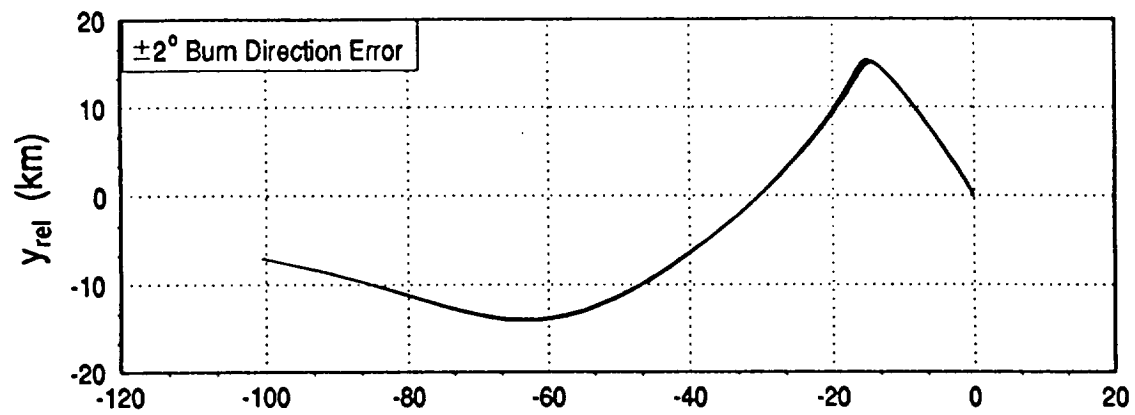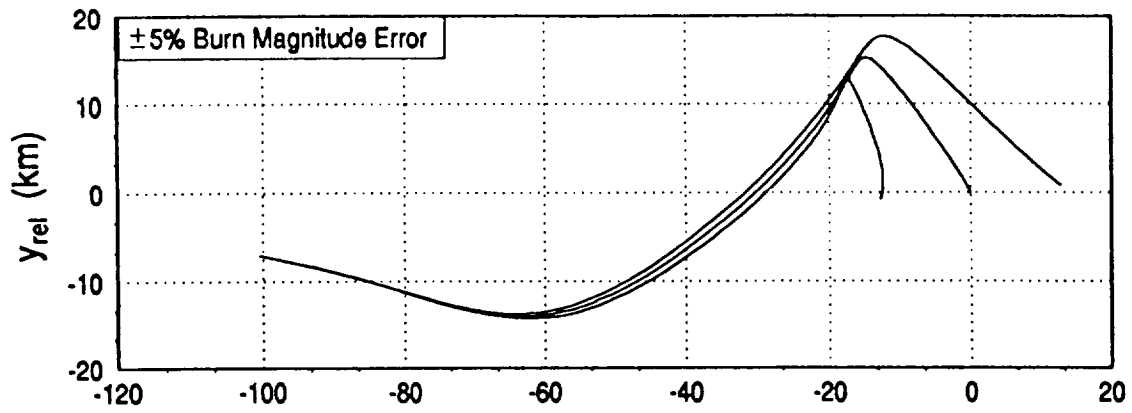Figure 3.17 Relative Motion for Burn Magnitude Error Insensitivity Point

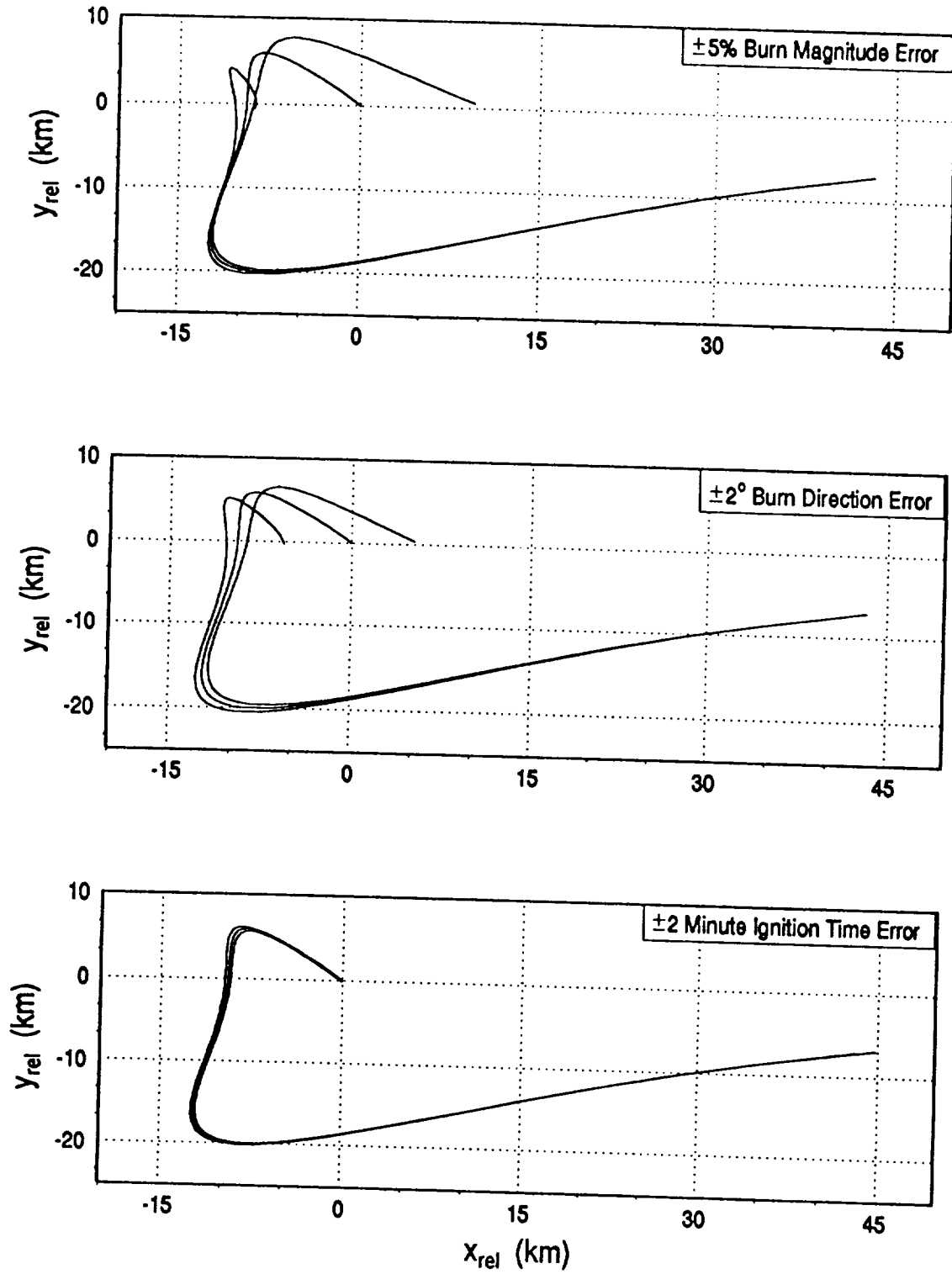Figure 3.18 Relative Motion for Burn Direction Error Insensitivity Point

Figure 3.19 Relative Motion for Ignition Time Error Insensitivity Point

Chapter 4

Navigation Error Tolerance

Any error in the estimate of the state of the chaser, either position or velocity or a combination of the two, will result in an error in the estimate of the required burn. If the expected error in the estimate of position as well as the relationship between the expected error in the estimate of velocity and the expected error in position can be identified, the state error vector becomes one-dimensional. The freedom obtained by allowing a small variation in the intercept time can then be used to develop maneuver point conditions which are robust to such one-dimensional errors due to state uncertainties.

4.1 Measurement Effects

The errors in a vehicle's estimation of its state relative to the target are determined by the instruments making the measurements. In many cases the instrumentation may give direct information in only one direction, and information must be inferred in the other directions. Sometimes this leads to families of states which are indistinguishable from a navigation point of view, because they result in essentially the same measurement history. Figure 4.1a shows an example of states that are indistinguishable with angular measurements, and Figure 4.1b, states that are indistinguishable with range measurements, at least in a low dynamics environment.
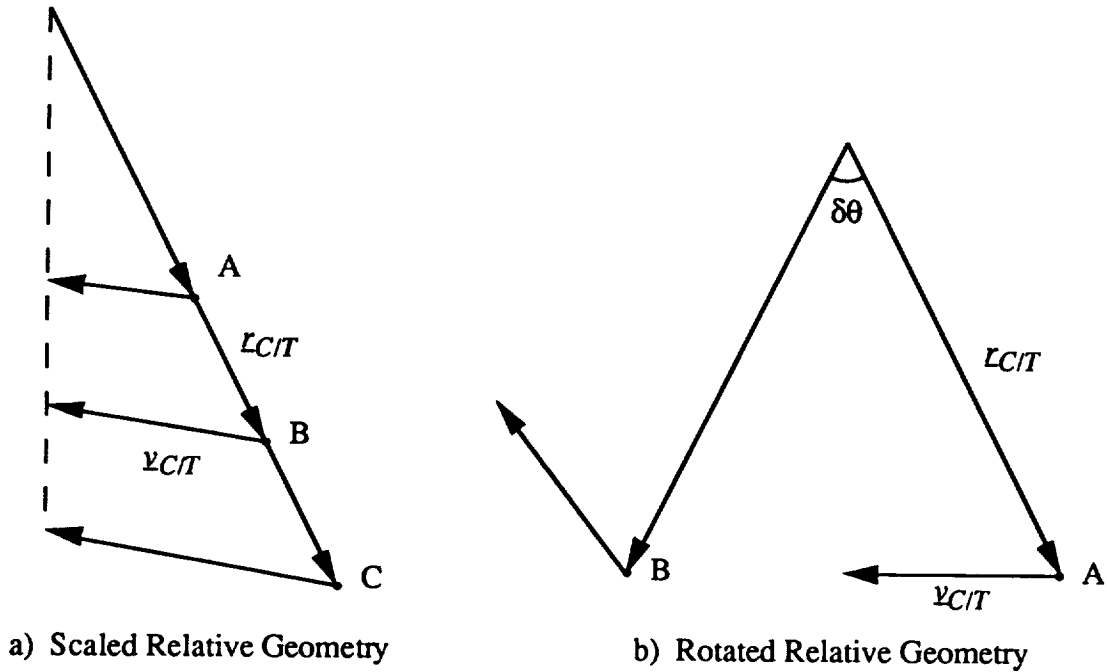
a) Scaled Relative Geometry

b) Rotated Relative Geometry

Figure 4.1 Indistinguishable Measurement Histories

4.2 Scaled Relative Geometry Error

During the early stages of rendezvous, the active vehicle may rely on "angles-only" navigation from star tracker measurements. The star tracker measurements supply direct information about the direction of the Line-of-Sight (LOS) from the chaser to the target. However, the chaser will have only very limited knowledge of its range along that LOS. Because of this, the relative state of the chaser will only be known within some scale factor. The error in estimated position of the chaser is primarily along the chaser's relative position vector. The error in estimated velocity is primarily along the relative velocity vector and the ratio of the velocity error to the position error is the same as the ratio of the relative velocity to the relative position. As Figure 4.2 shows,

$$\underline{r}_{act} = (1+\varepsilon)\underline{r}_{est} \Leftrightarrow \delta\underline{r} = \varepsilon\underline{r}_{est}$$

$$\underline{v}_{act} = (1+\varepsilon)\underline{v}_{est} \Leftrightarrow \delta\underline{v} = \varepsilon\underline{v}_{est} \tag{4.1}$$
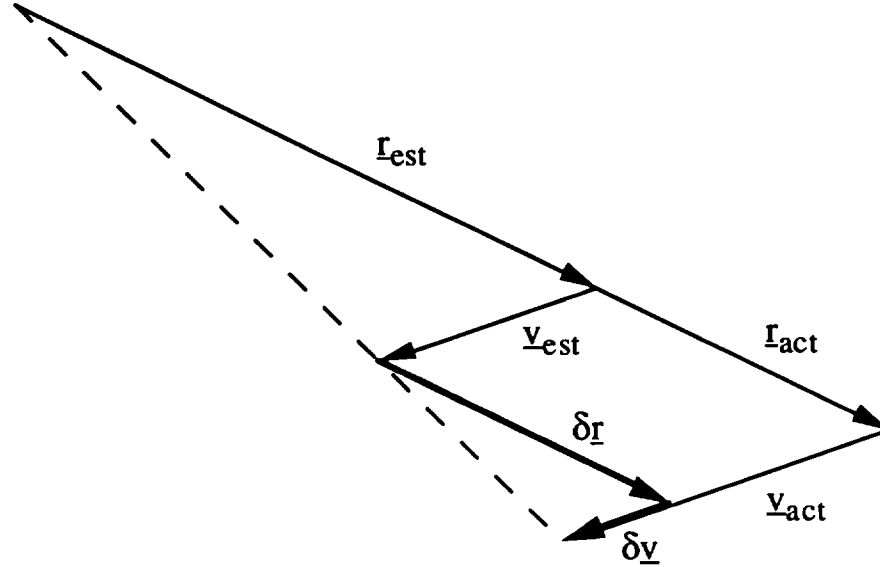

Figure 4.2 Scaled Relative Geometry Error

4.3 Rotated Relative Geometry Error

The vehicle may, instead, rely on radar measurements. These measurements supply direct information about the range from the chaser to the target, and the chaser will have only very limited knowledge of the direction of the LOS to the target. For small rotations, the error in estimated position of the chaser is primarily perpendicular to the chaser's relative position vector. Likewise, we may expect the error in estimated velocity to be perpendicular to the relative velocity. As Figure 4.3 shows,

$$\underline{r}_{act} = (I + \underline{u}x)\underline{r}_{est} \Leftrightarrow \delta\underline{r} = (\underline{u}x)\underline{r}_{est}$$

$$\underline{v}_{act} = (I + \underline{u}x)\underline{v}_{est} \Leftrightarrow \delta\underline{v} = (\underline{u}x)\underline{v}_{est} \tag{4.2}$$
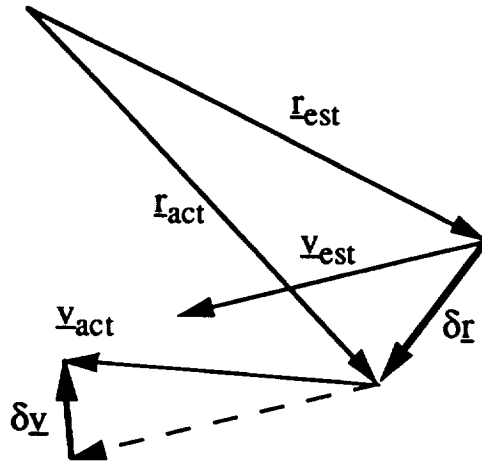
Figure 4.3 Rotated Relative Geometry Error

4.4 Covariance Analysis

To demonstrate that the scaled relative geometry relationship in Equation 4.1 does, in

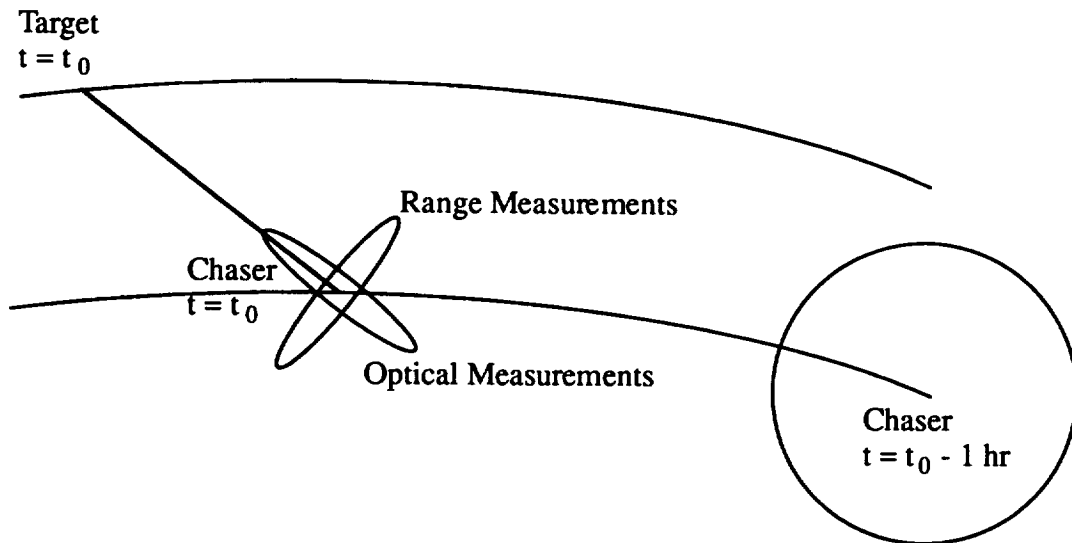fact, occur, a covariance analysis was used to generate representative statistics of state


Figure 4.4 Position Error Ellipses After One Hour of Measurements

errors through one hour of optical measurements. The target is in the highly elliptic orbit around Mars and the chaser is in the scaled elliptic staging orbit. The chaser starts with a large, diagonal covariance matrix (Figure 4.4). Correlations develop quickly, and Table 4.1 lists the results at the end of one hour of optical measurements[1].

		size and orientation of position error ellipse in $\underline{r}_{C/T}$ frame			size and orientation of velocity error ellipse in $\underline{v}_{C/T}^-$ frame		
f_C	f_T	a	b	ϕ	a	b	ϕ
45	45.9427	1327	9	-0.01	0.6840	0.0051	-0.82
135	135.4949	2256	26	-0.02	0.2154	0.0288	3.85
180	180.0474	8848	5	-0.00	0.3869	0.0167	0.10
225	225.0423	5003	1	0.00	0..5134	0..0023	-0.02
315	315.0552	1654	1	0.00	0.8142	0.0004	0.00

Table 4.1 Orientation of Position and Velocity Error Ellipses after One Hour Of Optical Navigation

---

[1] a is the semi-major axis, b is the semi-minor axis, and ϕ is the angle between the major axis and the chosen coordinate system .
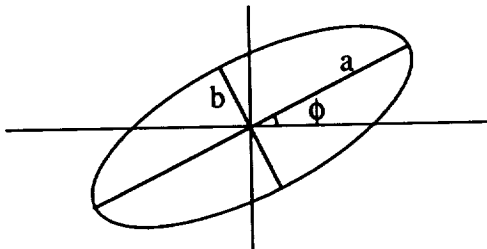
As expected, the long major axis of the equi-probability position error ellipse is essentially parallel to the relative position vector and the much shorter minor axis is perpendicular to it. The long major axis of the velocity error ellipse is essentially parallel to the relative velocity vector and the much shorter minor axis is perpendicular to it. Now that the direction of the estimation error has been identified, a maneuver point condition robust to errors due to optical measurements can be derived.

In contrast, the expected rotated relative geometry relationship of Equation 4.2 does not develop. The same covariance analysis was used to generate representative statistics of state errors through one hour of range measurements. Table 4.2 lists the results at the end of the hour of range measurements.

		size and orientation of position error ellipse in $r_{C/T}$ frame			size and orientation of velocity error ellipse in $v_{C/T}^-$ frame		
f_C	f_T	a	b	ϕ	a	b	ϕ
45	45.9427	59	19	83.33	0.0627	0.0043	-5.92
135	135.4949	2277	20	-89.99	0.4453	0.0079	-41.86
180	180.0474	13739	20	90.00	0.4317	0.0456	-7.56
225	225.0423	1302	20	89.99	0..1147	0..0167	54.79
315	315.0552	108	19	-87.36	0.0704	0.0076	-53.56

Table 4.2 Orientation of Position and Velocity Ellipses after One Hour Of Range Navigation

As expected, the position error is primarily perpendicular to the relative position vector.[2] Strong correlations do develop in the components of the velocity error, but not the correlations expected of a rotated relative geometry. The orbital dynamics are creating more complicated indistinguishable states. Before robust maneuver point conditions can be developed for this case, more work needs to be done to understand the velocity error correlations.

4.5 Scaled Relative Geometry Error -- Burn Magnitude Error Approximation

Error in the estimate of the position and velocity of the chaser will cause a post-burn velocity error which is, in general, a combination of burn magnitude error and burn direction error. Because we're using staging orbits of nearly the same size and shape as the target orbits, the difference between the state of the chaser and that of the target is fairly small. If the chaser's state can be treated as a perturbation of the target's state,

$$\underline{r}_C(t_0) = \underline{r}_T(t_0) + \delta \underline{r}(t_0)$$
$$\underline{v}_C(t_0) = \underline{v}_T(t_0) + \delta \underline{v}(t_0) \tag{4.3}$$

the chaser's state at some later time can be written as

$$\begin{bmatrix} \delta \underline{r}(t_1) \\ \delta \underline{v}(t_1) \end{bmatrix} = \Phi_K \begin{bmatrix} \delta \underline{r}(t_0) \\ \delta \underline{v}(t_0) \end{bmatrix} = \begin{bmatrix} K_1 & K_2 \\ K_3 & K_4 \end{bmatrix} \begin{bmatrix} \delta \underline{r}(t_0) \\ \delta \underline{v}(t_0) \end{bmatrix} \tag{4.4}$$

---

[2]The cases which passed through regions of higher orbital dynamics ($f_C = 45°$ and also $f_C = 315°$) have gained significant information in both directions (a and b are both small).

$$K_1 \equiv \frac{\partial \underline{r}(t_1)}{\partial \underline{r}(t_0)} \qquad K_2 \equiv \frac{\partial \underline{r}(t_1)}{\partial \underline{v}(t_0)}$$

$$K_3 \equiv \frac{\partial \underline{v}(t_1)}{\partial \underline{r}(t_0)} \qquad K_4 \equiv \frac{\partial \underline{v}(t_1)}{\partial \underline{v}(t_0)}$$

In order for the chaser to intercept the target, the final deviation of the chaser position from the target position must be zero. Using this to solve for the deviation from target velocity required to achieve intercept,

$$\delta \underline{v}_{req} = -K_2^{-1} K_1 \delta \underline{r}(t_0) \tag{4.5}$$

The burn required for intercept is

$$\Delta \underline{v}_{req} = \delta \underline{v}_{req} - \delta \underline{v}(t_0) \tag{4.6}$$

In reality, the chaser's relative position and velocity are only known within a scale factor. The actual position and velocity deviations are some small fraction larger or smaller than estimated:

$$\delta \underline{r}(t_0)_{act} = (1 + \varepsilon) \delta \underline{r}(t_0)_{est}$$
$$\delta \underline{v}(t_0)_{act} = (1 + \varepsilon) \delta \underline{v}(t_0)_{est} \tag{4.7}$$

The actual required velocity deviation is

$$\begin{aligned}
\left(\delta \underline{v}_{req}\right)_{act} &= -K_2^{-1} K_1 \delta \underline{r}(t_0)_{act} \\
&= -K_2^{-1} K_1 (1 + \varepsilon) \delta \underline{r}(t_0)_{est} \\
&= (1 + \varepsilon)\left(\delta \underline{v}_{req}\right)_{est}
\end{aligned} \tag{4.8}$$

and the actual burn required is

$$\left(\Delta \underline{v}_{req}\right)_{act} = \left(\delta \underline{v}_{req}\right)_{act} - \delta \underline{v}(t_0)_{act}$$
$$= (1+\varepsilon)\left(\delta \underline{v}_{req}\right)_{est} - (1+\varepsilon)\delta \underline{v}(t_0)_{est}$$
$$= (1+\varepsilon)\left(\Delta \underline{v}_{req}\right)_{est} \tag{4.9}$$

Scaled relative geometry results in a scaled required velocity and a scaled required burn (Figure 4.5). The estimate of the required burn is correct in direction, but wrong in magnitude. This scaled relative geometry error can be treated as a burn magnitude error and the previously developed condition (Equation 3.3) applies.
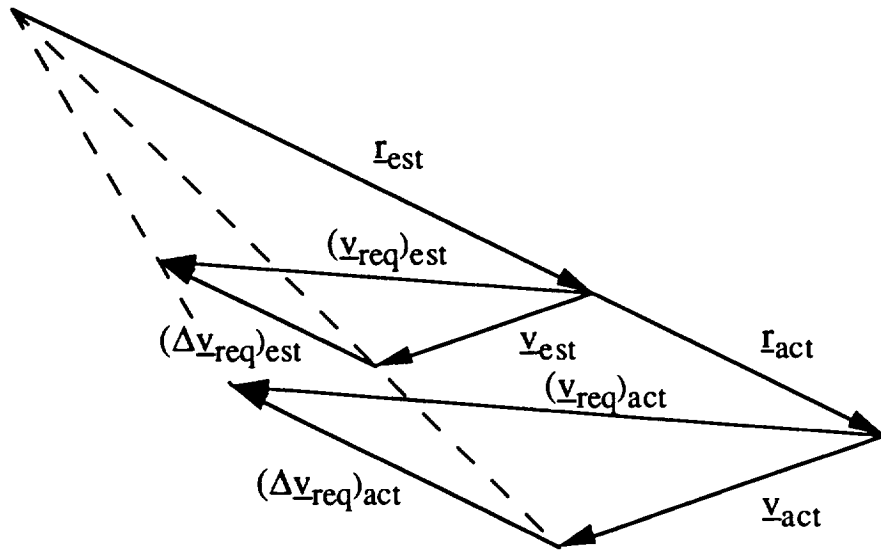
Figure 4.5 Scaled Relative Geometry Error Results in Burn Magnitude Error

4.6 Scaled Relative Geometry Error -- Maneuver Point Condition

When the state of the chaser cannot be treated as a deviation from the state of the target, the previous applied method can be used to develop a more general form of the maneuver point condition which provides insensitivity to scaled relative geometry errors.

$$\delta(\Delta \underline{v}_{req}) = \underline{\lambda}_0 \delta \Delta t + L_1 \delta \underline{r}_C(t_0) + L_2 \delta \underline{r}_T(t_1) - \delta \underline{v}_C^-(t_0) \qquad (2.3b)$$

The error in the estimated position of the chaser is in the direction of the relative position vector with a magnitude which is some fraction of that of the relative position vector. The error in the estimated velocity is in the direction of the relative velocity vector and its magnitude the same fraction of the magnitude of the relative velocity.

$$\delta \underline{r}_C(t_0) = \varepsilon\left(\underline{r}_C(t_0) - \underline{r}_T(t_0)\right) = \varepsilon \underline{r}_{C/T}(t_0)$$
$$\delta \underline{v}_C^-(t_0) = \varepsilon\left(\underline{v}_C^-(t_0) - \underline{v}_T(t_0)\right) = \varepsilon \underline{v}_{C/T}^-(t_0) \qquad (4.10)$$

Since transfer time and final position of the target do not change, the change in required burn due to a scaled relative geometry error is

$$\delta(\Delta \underline{v}_{req}) = \varepsilon\left(L_1 \underline{r}_{C/T}(t_0) - \underline{v}_{C/T}^-(t_0)\right) \qquad (4.11a)$$

For convenience, we define

$$\underline{w}_s \equiv L_1 \underline{r}_{C/T}(t_0) - \underline{v}_{C/T}^-(t_0)$$

$$\delta(\Delta \underline{v}_{req}) = \varepsilon \underline{w}_s \qquad (4.11b)$$

In order for rendezvous to occur, this deviation in required burn combined with the deviation in required burn associated with a deviation in time of intercept must be zero.

$$\delta(\Delta \underline{v}_{req}) = \underline{w}_{t_1} \delta t_1 + \varepsilon \underline{w}_s = \underline{0}$$
$$\underline{w}_{t_1} \delta t_1 = -\varepsilon \underline{w}_s \qquad (4.12)$$

The condition for insensitivity to a scaled relative geometry error is

$$\underline{w}_s \times \underline{w}_{t_1} = \underline{0} \qquad (4.13)$$

Equation 4.13 is the maneuver point condition which provides insensitivity to scaled relative geometry error.

The corresponding variation in time of intercept is

$$\delta t_1 = -\varepsilon \frac{\underline{w}_s \cdot \underline{w}_{t_1}}{\underline{w}_{t_1} \cdot \underline{w}_{t_1}} = \pm \varepsilon \frac{|\underline{w}_s|}{|\underline{w}_{t_1}|} \qquad (4.14)$$

4.7 Deterministic Results

Figure 4.6 shows the solutions for the burn magnitude error approximation and the more general scaled relative geometry maneuver point condition. In the case of the circular rendezvous, the results which are almost indistinguishable. However the two sets of results for the scaled elliptic and coelliptic rendezvous appear to be quite different (Figures 4.7 and 4.8).

Even though the burn magnitude approximation is not exactly the same as the scaled relative geometry maneuver point condition, the difference is not necessarily significant. Because the scaled relative geometry error primarily causes a burn magnitude error, maneuver points which are insensitive to one type of error are fairly tolerant of the other type.
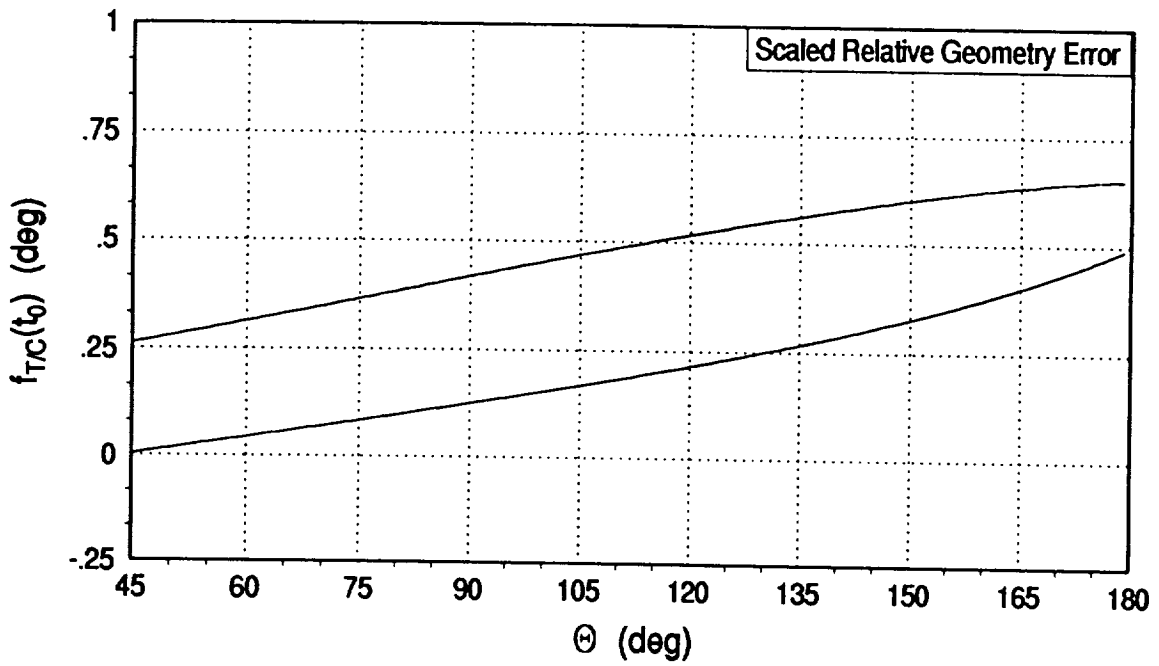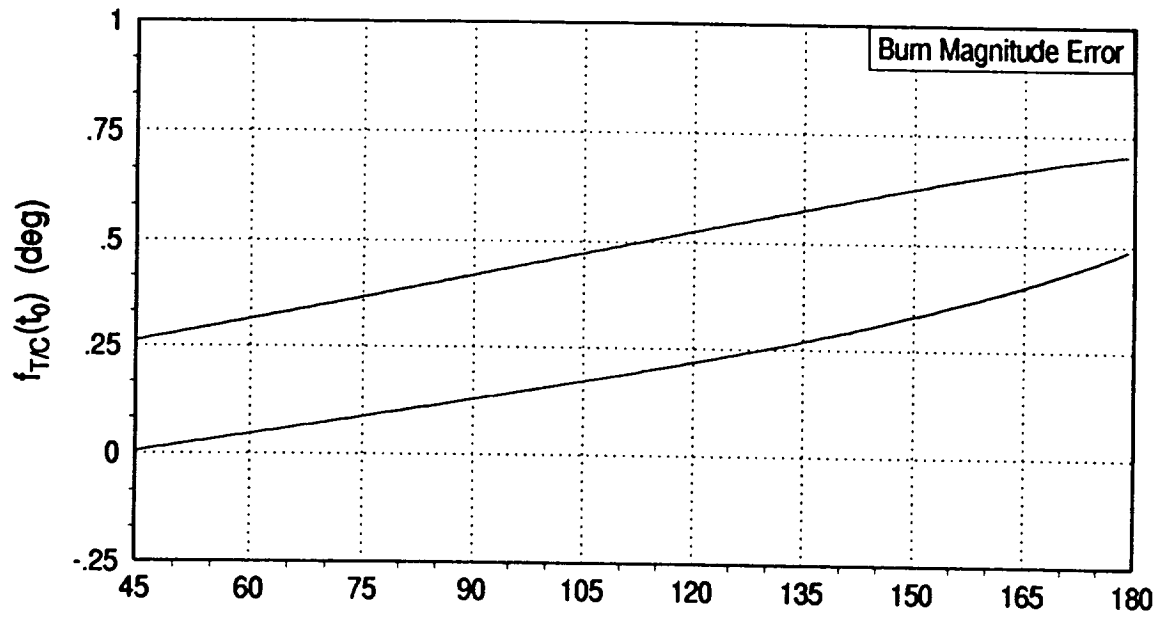
Figure 4.6 Comparison of Burn Magnitude Error and Scaled Relative Geometry Error
Insensitivity Points for Cocircular Staging Orbit
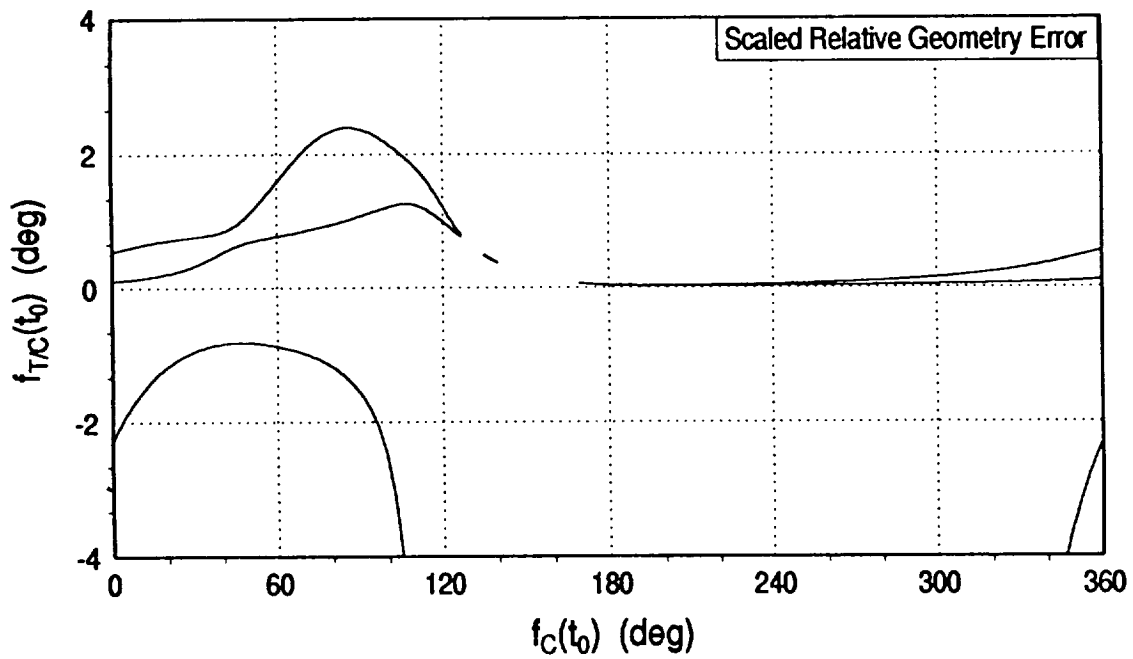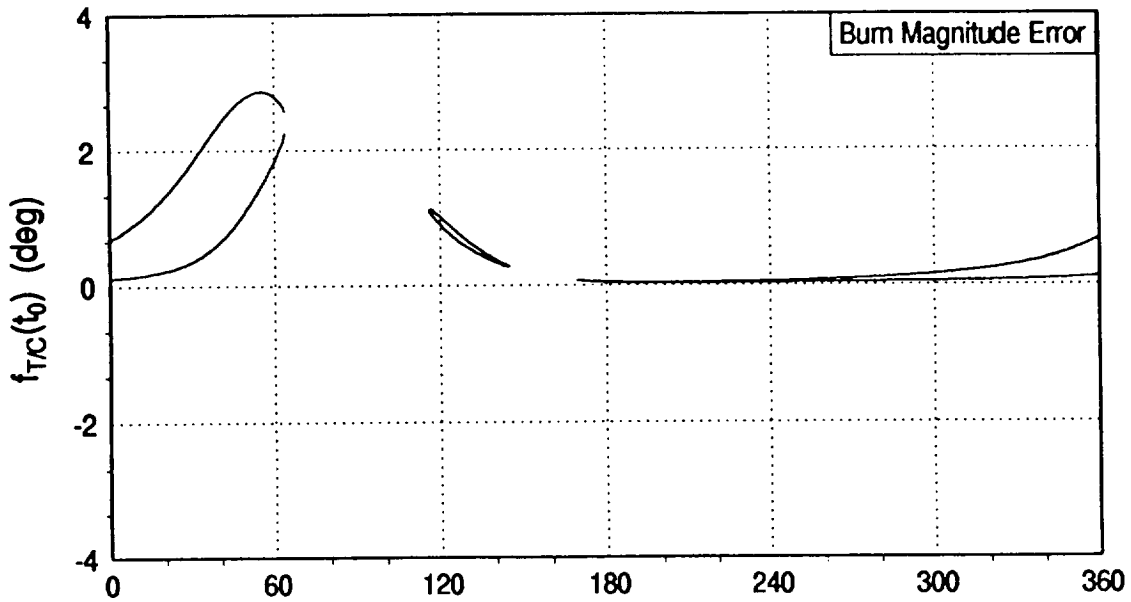
Figure 4.7 Comparison of Burn Magnitude Error and Scaled Relative Geometry Error

Insensitivity Points for Scaled Elliptic Staging Orbit
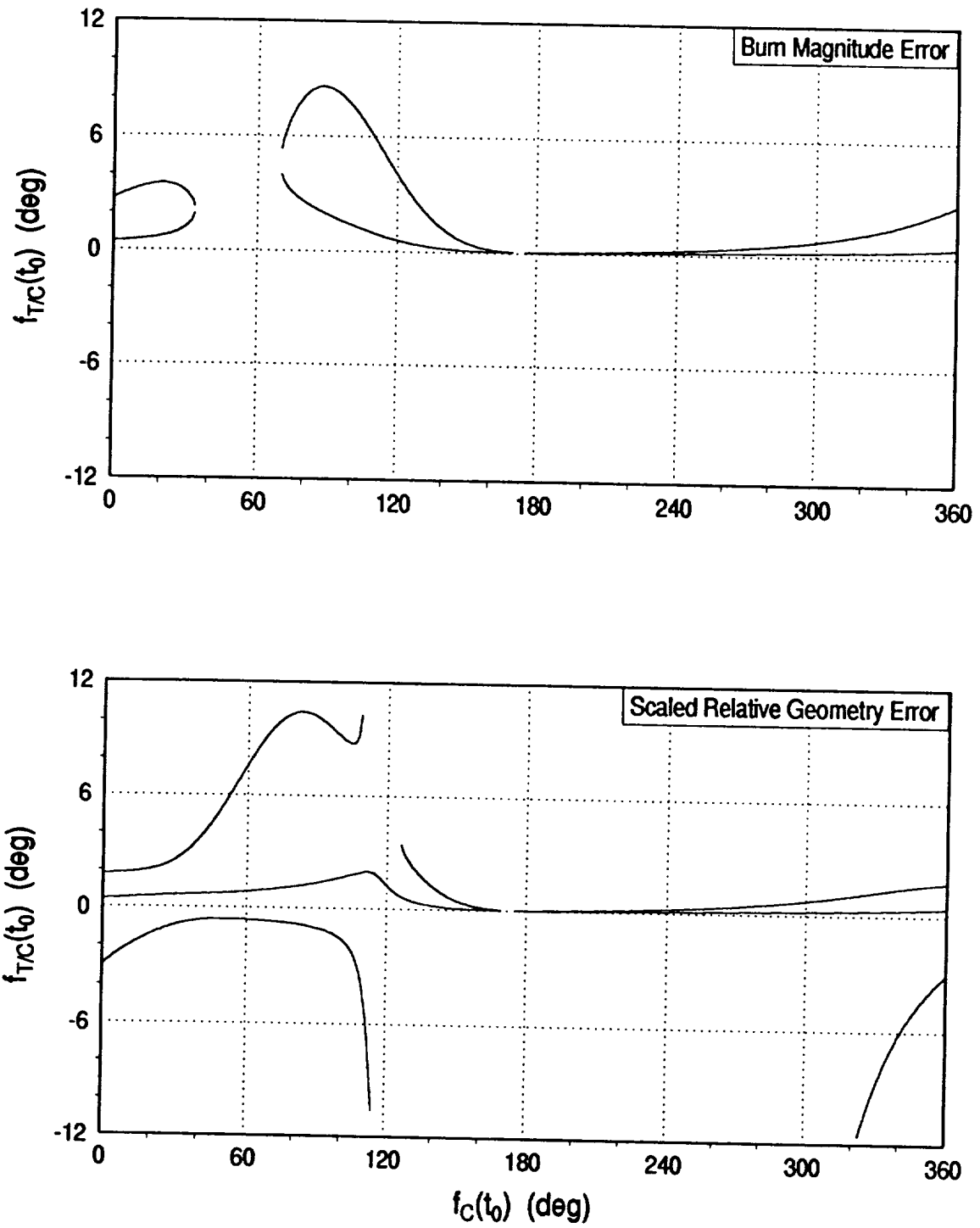
Figure 4.8 Comparison of Burn Magnitude Error and Scaled Relative Geometry Error
Insensitivity Points for Coelliptic Staging Orbit

The relative motion plots for transfer from one scaled relative geometry error insensitivity point (($f_c(t_0)$=90° and $f_{T/c}(t_0)$=1.07079° from Figure 4.7b) is shown in Figure 4.9.

4.8 Monte Carlo Analysis

The covariance matrices found in Section 4.4 were used to generate ten representative state dispersions around five navigation insensitivity points. These "actual" states were then propagated forward to rendezvous. Figures 4.11 through 4.15 show the relative motion plots from dispersed initial states for both optical and range measurements.
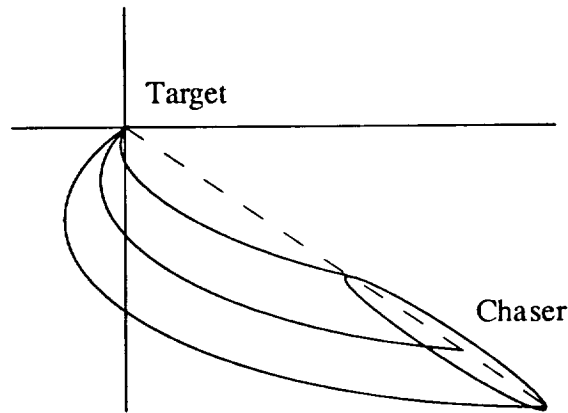
Figure 4.10 Monte Carlo Analysis

In the optical case, the pure scaled relative geometry portion of the error is fully compensated for by the appropriate choice of maneuver point. This leaves a much smaller initial burn error which causes a much smaller final position error. In Figure 4.12, the dispersed states do not converge as well at rendezvous. This is the case in Section 4.4 where the scaled relative geometry had not fully developed during the one hour allotted.
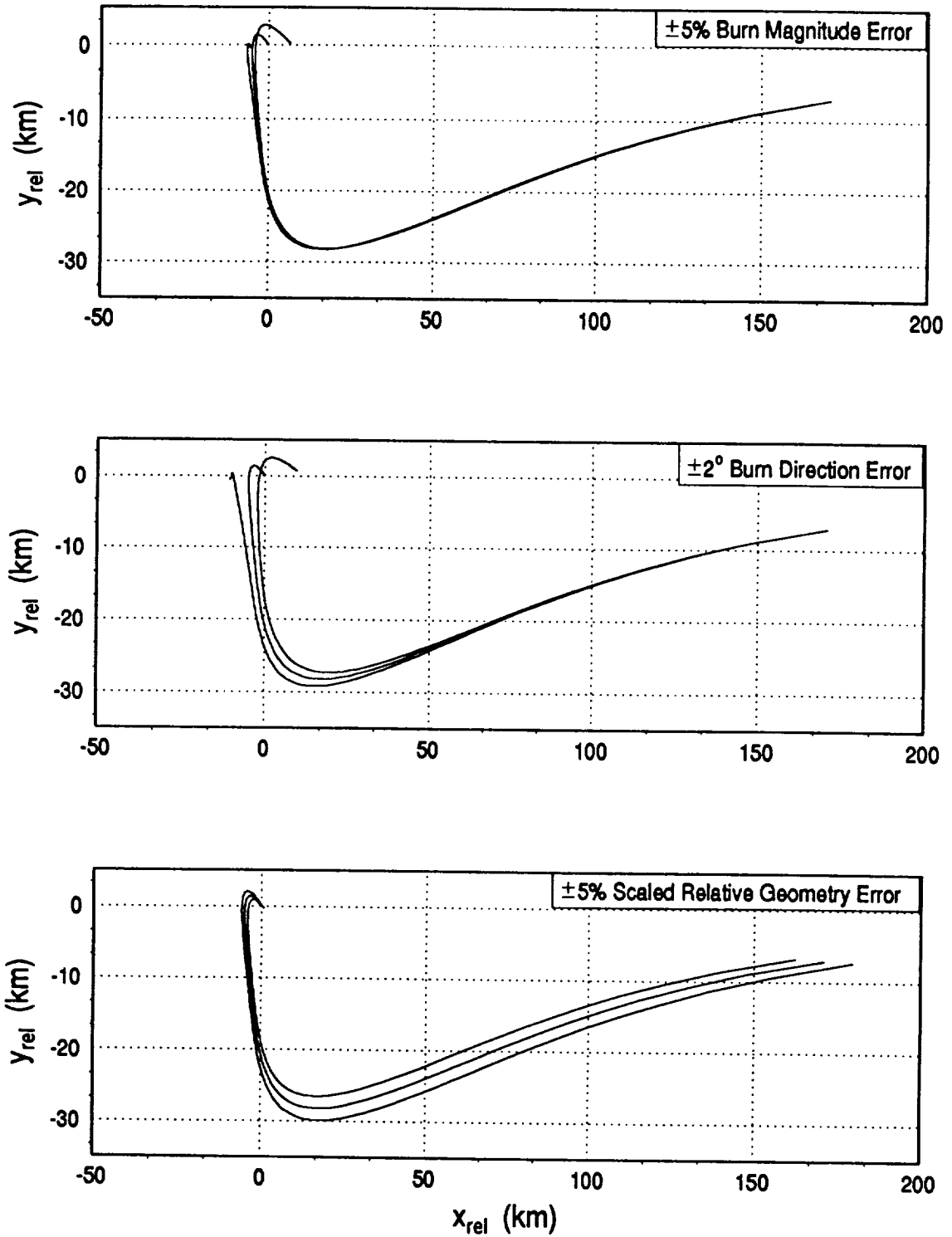
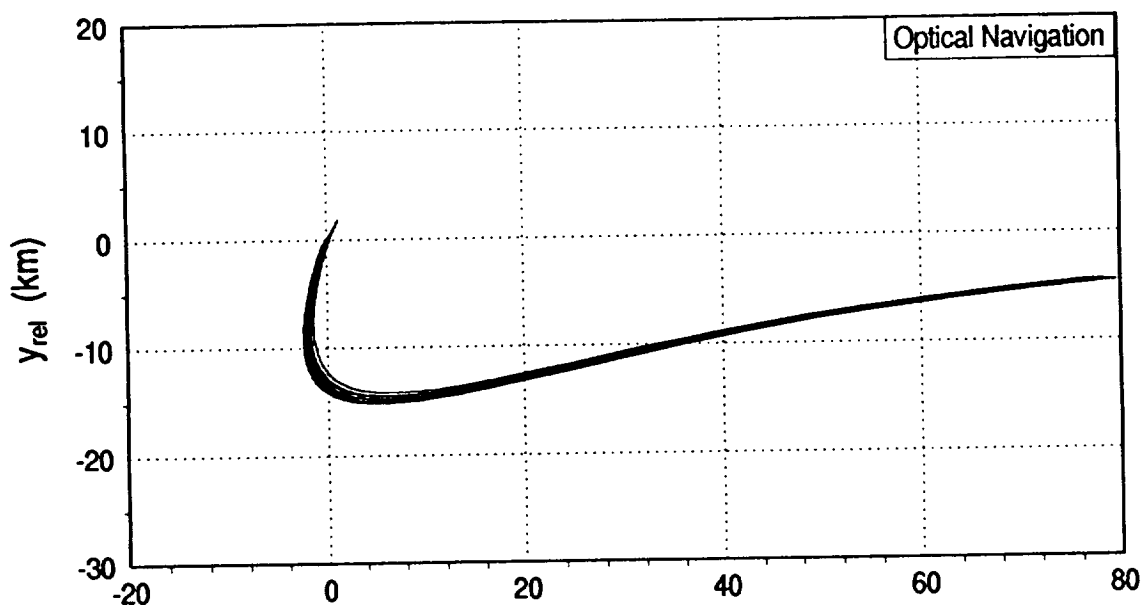Figure 4.9 Relative Motion Plots for Scaled Relative Geometry Insensitivity Point
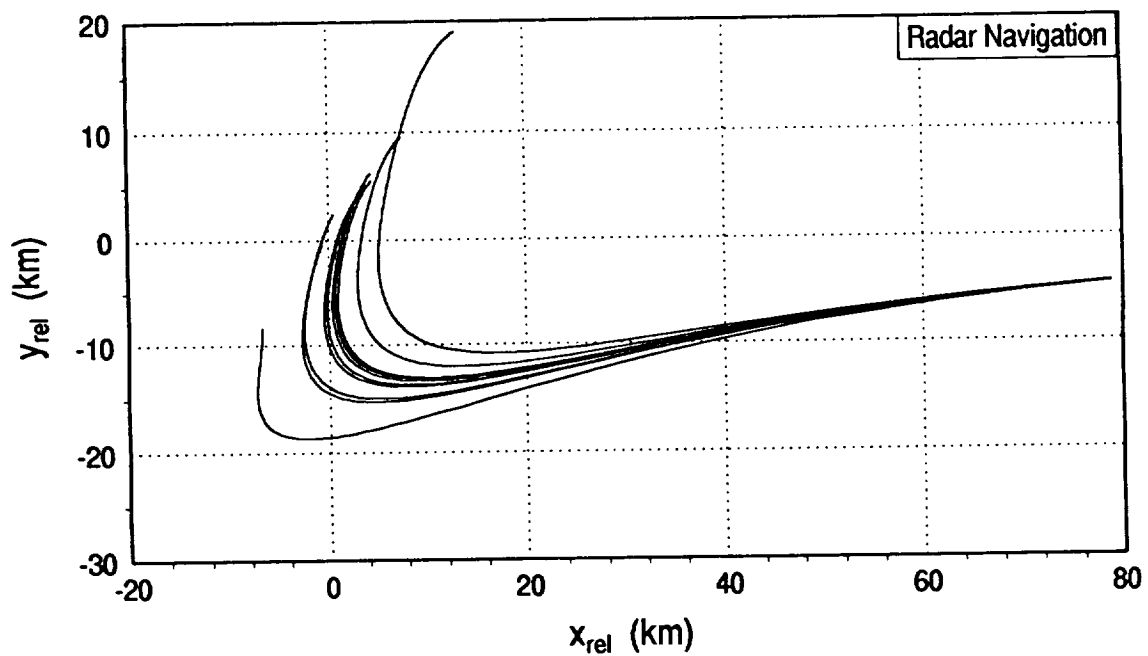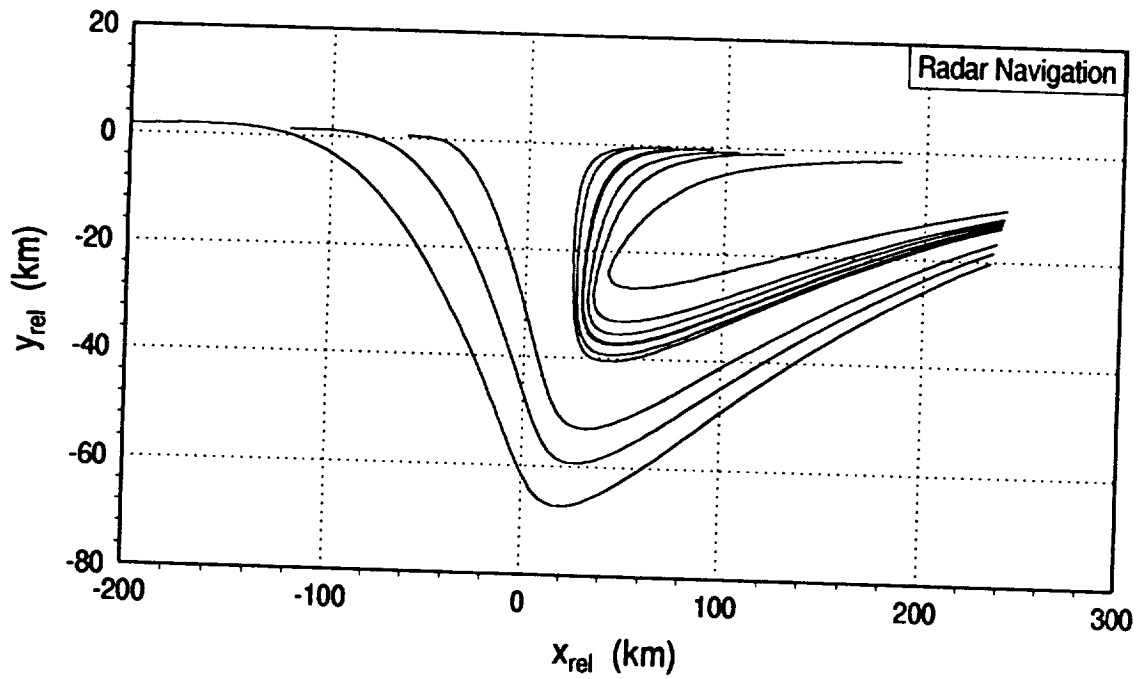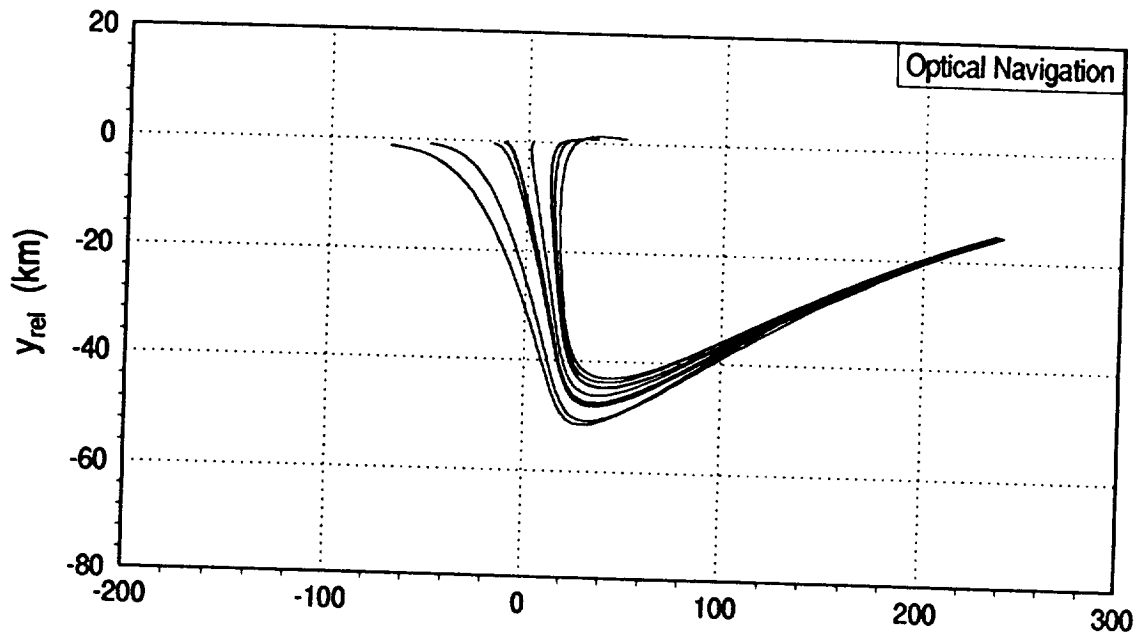
Figure 4.11 Dispersed States - $f_c(t_0)=45°$
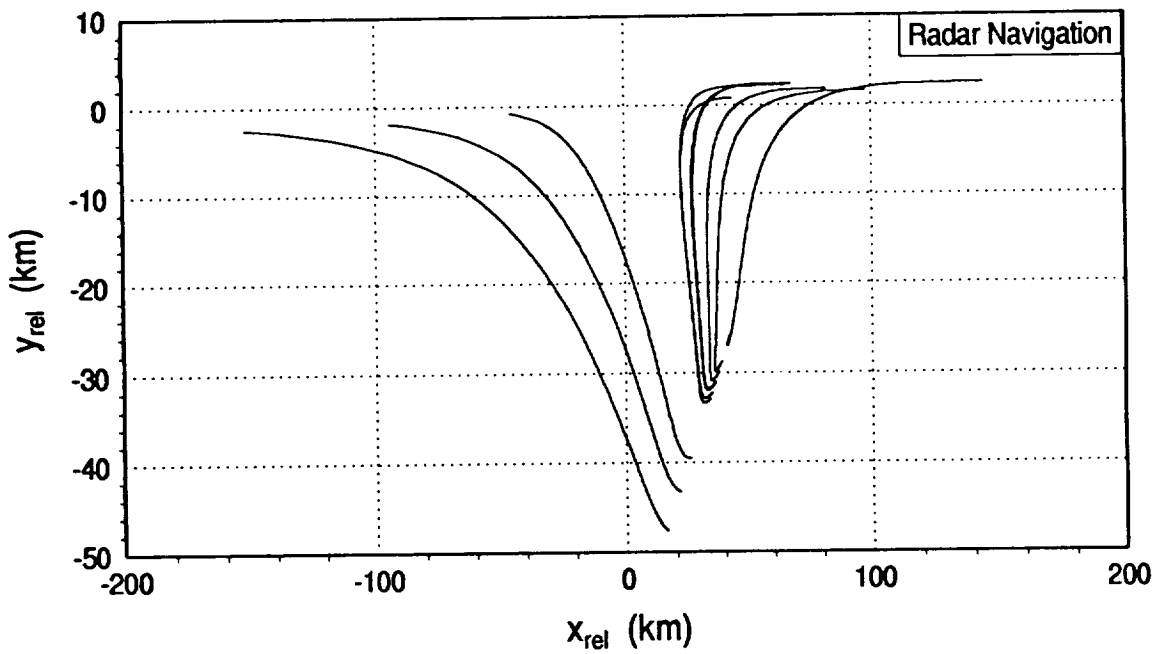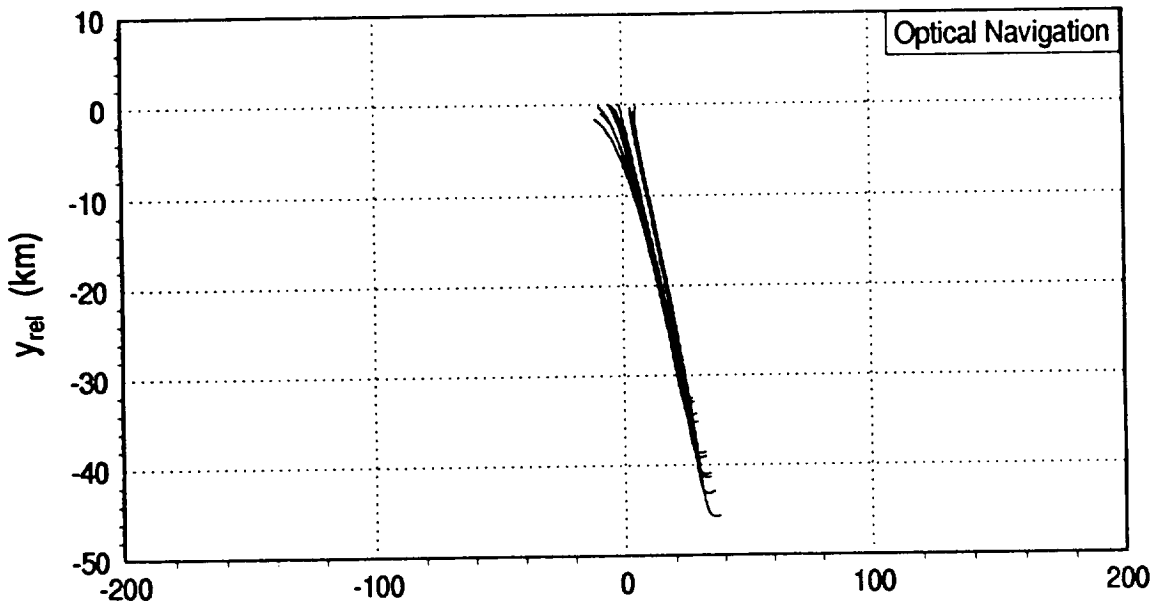
Figure 4.12 Dispersed States - $f_c(t_0)$=135°
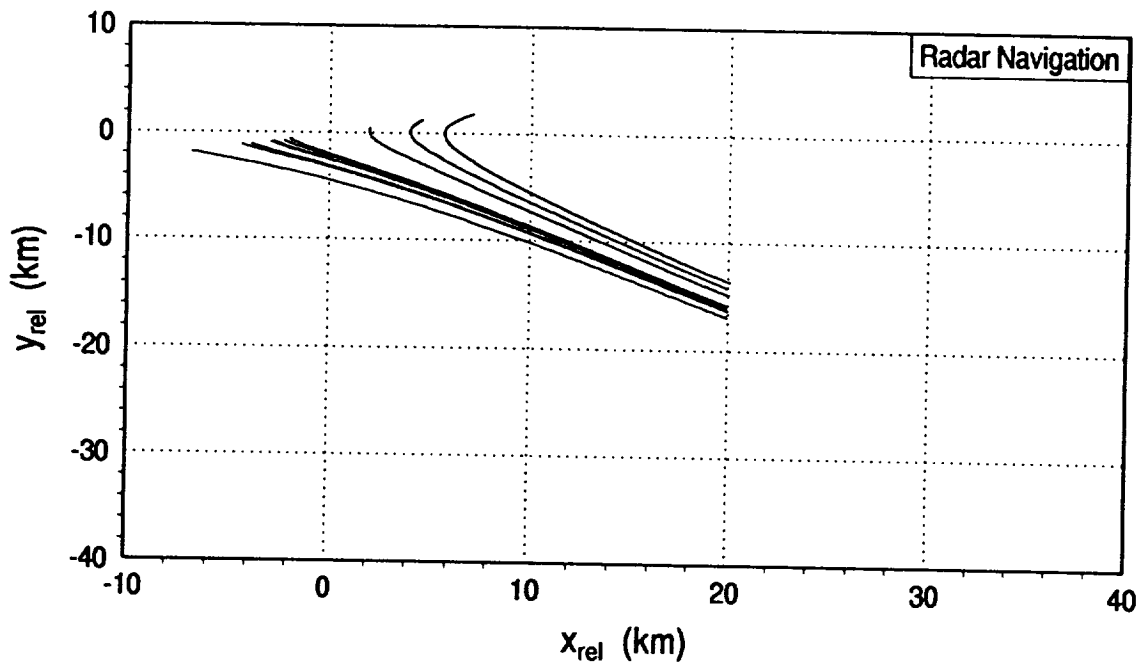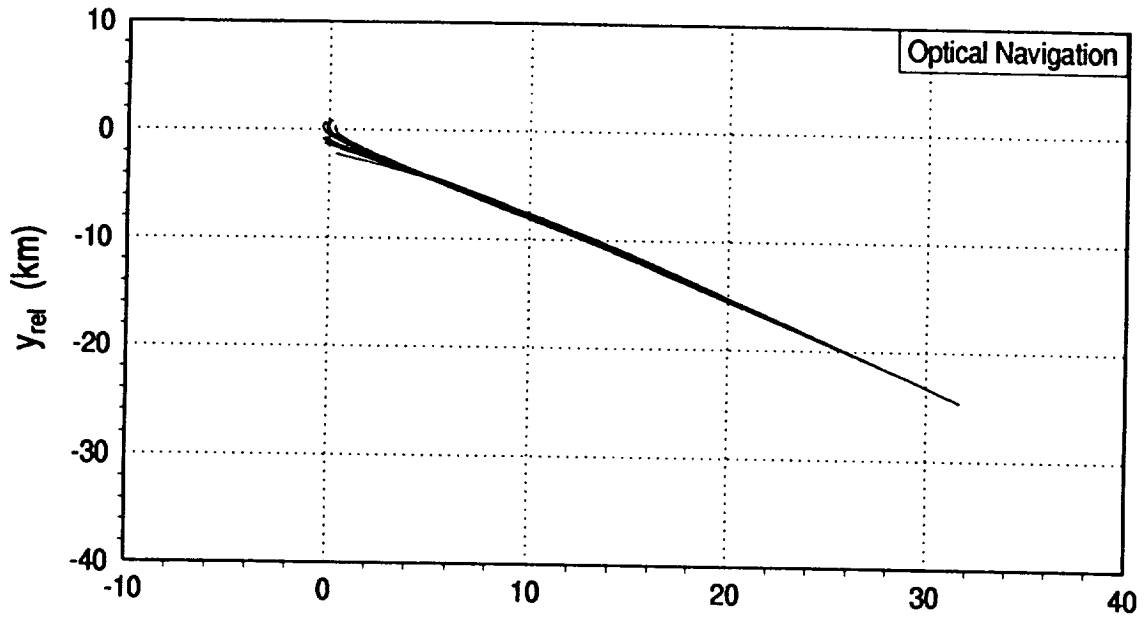
Figure 4.13 Dispersed States - $f_c(t_0)=180°$

71

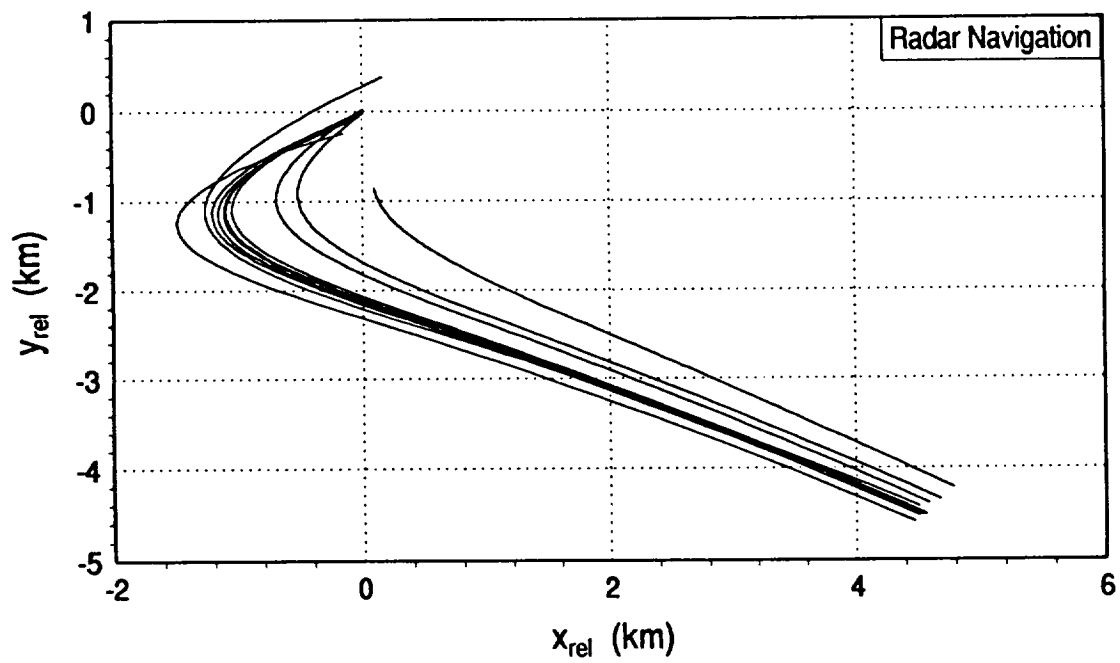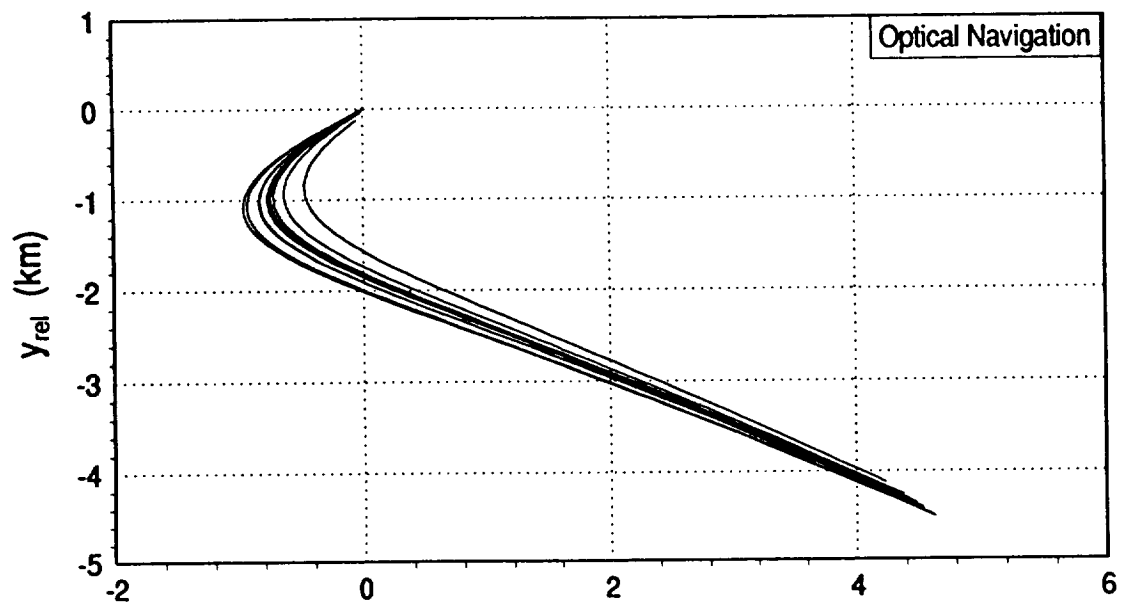Figure 4.14 Dispersed States - $f_c(t_0)$=225°

Figure 4.15 Dispersed States - $f_c(t_0)=315°$

Chapter 5

Conclusions

5.1 Summary of Results

The purpose of this thesis has been to develop maneuver point conditions which determine transfer phases robust to errors in burn execution and navigation. Chapter 2 identified the degree of freedom gained by allowing a small variation in time of intercept and noted the restrictions placed upon use of this freedom by linearity assumptions. Chapters 3 and 4 showed that in cases where one dimensional errors in burn execution and navigational uncertainties can be aligned with the degree of freedom, the rendezvous will still occur, albeit at a slightly different time. Such insensitivity points can be applied to both circular and highly elliptic orbits and still maintain reasonable times of transfer and fuel consumption. In cases where the error of concern is never perfectly aligned with the degree of freedom, no maneuver points exist . However, in such cases, the maneuver points where the error and the allowable error come closest to alignment provide the most tolerance of that particular error. In general, for any one-dimensional error, the possible transfers can be searched for regions where the error and the allowable error come closest to alignment. These regions will provide a measure of robustness for that error.

5.2 Future Research

This thesis developed a set of robust maneuver point conditions, and in doing so raised many questions. Can we establish conditions for the existence of solutions? If solutions do exist, how many exist? Why do we have three solution points in some regions for insensitivity to scaled relative geometry errors when there are only two or no solution points for insensitivity to any of the three burn execution errors?

These maneuver points are only valid as long as the linearity assumptions are not violated. If the anticipated errors will necessitate time slips and vehicle motion beyond the region of linearity second order effects might be included to expand this region of linearity.

This thesis applied the robust maneuver point conditions to circular and highly elliptic orbits. Further studies should investigate the range of orbit eccentricities and of central transfer angles. The relative size and orientation of the chaser orbit (angular difference in the line of apsides) will also effect the solution space. In addition, more complicated phasing orbits, such as those used in Shuttle missions should be investigated. The analysis will also vary slightly if the transition is to a station keeping point near, but away from, the target. This study could be expanded to direct rendezvous, i.e., no intermediate staging orbit. These conditions may even be applicable to rendezvous with a target in a hyperbolic orbit.

Another area of research involves the identification of state uncertainties resulting from range measurements. While the position error is clearly perpendicular to the relative position vector, the relationship of the velocity error to this position error has not been identified. It may be that the dynamics of the orbit, coupled with the higher order terms,

may yield further information concerning this relationship. Any other expected state errors that develop while taking other types of measurements (or combinations of measurements) should also be investigated.

Armed with this method, the mission planner can locate robust maneuver points that balance other mission constraints such as fuel expenditure, closing velocities, and final approach geometries. Out-of-plane errors should be examined in future studies. In addition, the perturbation effects due to central body oblateness, atmospheric drag, and the gravitational attraction of the Sun should not be ignored. Further research in these areas and others is required if the mission to Mars is to become a reality.

Appendix A

Alternate Forms of the Maneuver Point Conditions

A.1 Determination of Freedom in Final Relative Position

The final position of the chaser is a function of the transfer time involved and the initial position and velocity of the chaser:

$$\underline{r}_C(t_1) = f\big(\Delta t, \underline{r}_C(t_0), \underline{v}_C^+(t_0)\big)$$

If there are deviations in any of these variables, the final position of the chaser changes:

$$\delta \underline{r}_C(t_1) = \frac{\partial \underline{r}_C(t_1)}{\partial \Delta t} \delta \Delta t + \frac{\partial \underline{r}_C(t_1)}{\partial \underline{r}_C(t_0)} \delta \underline{r}_C(t_0) + \frac{\partial \underline{r}_C(t_1)}{\partial \underline{v}_C^+(t_0)} \delta \underline{v}_C^+(t_0)$$

or more compactly,

$$\delta \underline{r}_C(t_1) = \underline{v}_C^-(t_1) \delta \Delta t + K_1 \delta \underline{r}_C(t_0) + K_2 \delta \underline{v}_C^+(t_0)$$

Specifically, if we allow a small perturbation in total transfer time, δt, the initial position and velocity of the active vehicle do not change. The final position deviations of the the active and passive vehicles are

$$\delta \underline{r}_C(t_1) = \underline{v}_C^-(t_1) \delta t_1$$

$$\delta \underline{r}_T(t_1) = \underline{v}_T(t_1) \delta t_1$$

The difference between these two final position deviations is the deviation in final relative position of caused by the small slip in total transfer time

$$\delta \underline{r}_C(t_1) - \delta \underline{r}_T(t_1) = \left(\underline{v}_C^-(t_1) - \underline{v}_T(t_1) \right) \delta t_1 \tag{A.1}$$

This is the direction of freedom in final relative position. Small errors in final relative position which are aligned with the relative velocity are absorbed as small variations in transfer time. Those which are perpendicular remain as pure miss distance.

A.2 Magnitude and Direction Errors

There is no deviation in initial position or pre-burn velocity of the chaser associated with a pure burn magnitude or direction error.

An error in burn magnitude, $\delta(\Delta \underline{v})_\parallel \equiv \varepsilon \Delta \underline{v}_{req}$, causes an error in the final position of the chaser:

$$\delta \underline{r}_C(t_1) = \varepsilon K_2 \Delta \underline{v}_{req}$$

If this final position error happens to be aligned with the final relative velocity, the maneuver point provides some measure of insensitivity to this type of burn error:

$$K_2 \left(\Delta \underline{v}_{req} \right) \times \left(\underline{v}_C^-(t_1) - \underline{v}_T(t_1) \right) = \underline{0} \tag{A.2}$$

80

An in-plane error in burn direction, $\delta(\Delta\underline{v})_\perp \equiv \left(\Delta\underline{v}_{req} \times \underline{i}_h\right)\delta\theta$, causes an error in the final position of the chaser:

$$\delta\underline{r}_C(t_1) = K_2\left(\Delta\underline{v}_{req} \times \underline{i}_h\right)\delta\theta$$

If this happens to be aligned with the final relative velocity, the maneuver point provides some measure of insensitivity to this type of burn error:

$$K_2\left(\Delta\underline{v}_{req}\right)\cdot\left(\underline{v}_C^-(t_1) - \underline{v}_T(t_1)\right) = \underline{0} \tag{A.3}$$

A.3 Ignition Time Error

If we delay execution of the burn by some small amount of time, δt_0, the chaser's initial state, both position and pre-burn velocity, will change slightly.

$$\delta\underline{r}_C(t_0) = \underline{v}_C^-(t_0)\delta t_0$$
$$\delta\underline{v}_C^-(t_0) = \underline{g}_C(t_0)\delta t_0 = -\frac{\mu}{\left|\underline{r}_C(t_0)\right|^3}\underline{r}_C(t_0)\delta t_0$$

Because of this delay, we have less time to arrive at the nominal intercept point:

$$\delta\Delta t = -\delta t_0$$

Therefore, the deviation in the final position of the chaser is

$$\delta\underline{r}_C(t_1) = \left[-\underline{v}_C^-(t_1) + K_1\underline{v}_C^-(t_0) + K_2\underline{g}_C(t_0)\right]\delta t_0$$

In order for rendezvous to occur, this deviation in final position combined with the deviation in final relative position associated with a deviation in time of intercept must be zero.

$$\left[-\underline{v}_C^-(t_1) + K_1 \underline{v}_C^-(t_0) + K_2 \underline{g}_C(t_0)\right]\delta t_0 + \left[\underline{v}_C^-(t_1) - \underline{v}_T(t_1)\right]\delta t_1 = \underline{0}$$

For this to be true, the two vectors must be parallel or anti-parallel:

$$\left[-\underline{v}_C^-(t_1) + K_1 \underline{v}_C^-(t_0) + K_2 \underline{g}_C(t_0)\right] \times \left(\underline{v}_C^-(t_1) - \underline{v}_T(t_1)\right) = \underline{0} \tag{A.4}$$

Equations A.2, A.3, and A.4 are the maneuver point conditions which provide insensitivity to burn magnitude, direction, and ignition time errors. They are equivalent to those developed in Chapter 3.

Appendix B

Other Mission Constraints

Once the valid maneuver points have been identified other mission constraints can be used to make the final choice of transfer. Fuel expenditure will always be an important constraint. Closing velocity should be minimized for safety and control. Of course, when fuel expenditure is constrained, closing velocity tends to follow. The final approach angle should be chosen so that the target is against a dark background above the chaser. Plots for these three constraints are presented below, but similar plots should be made for each constraint of importance and consulted when making the final choice of transfer conditions.

See figures B.1a-c for fuel expenditure, closing velocity, and approach angle corresponding to the insensitive maneuver points for the cocircular Earth orbits.

See figures B.2a-c and B.3a-c for fuel expenditure, closing velocity, and approach angle corresponding to the coelliptic and the scaled elliptic staging orbits.
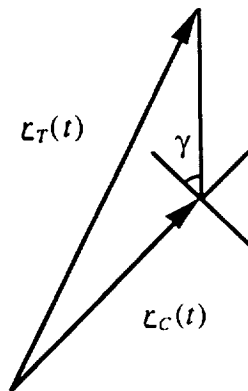
Figure B.1 LVLH Elevation Angle of LOS to Target
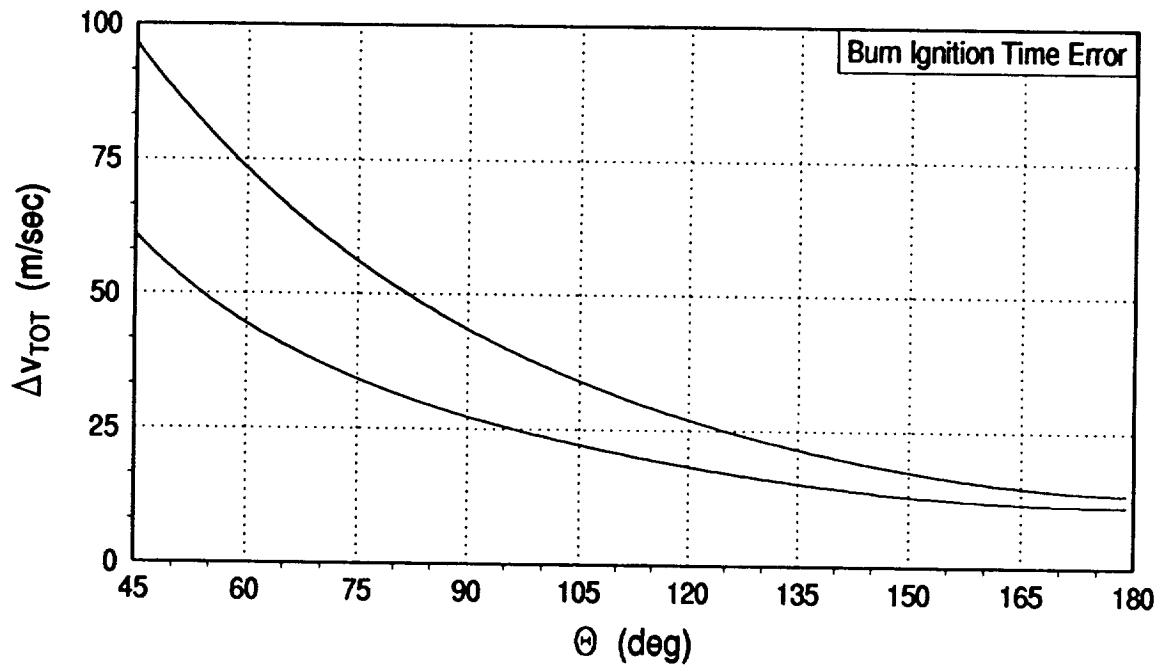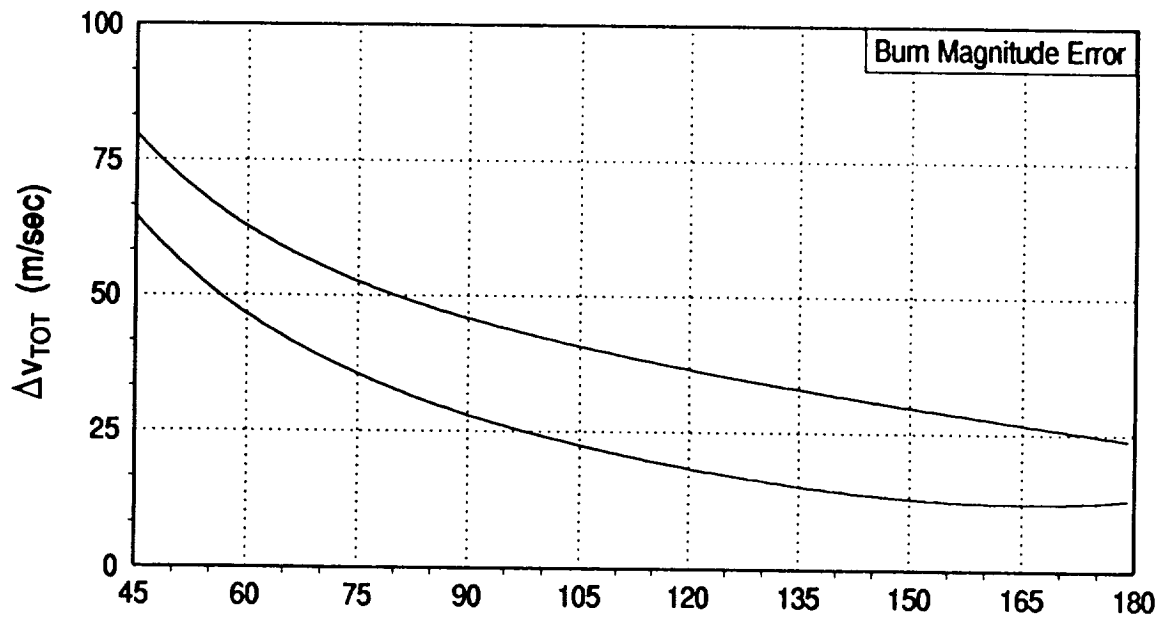
Figure B.2a Fuel Expenditure - Cocircular Staging Orbit
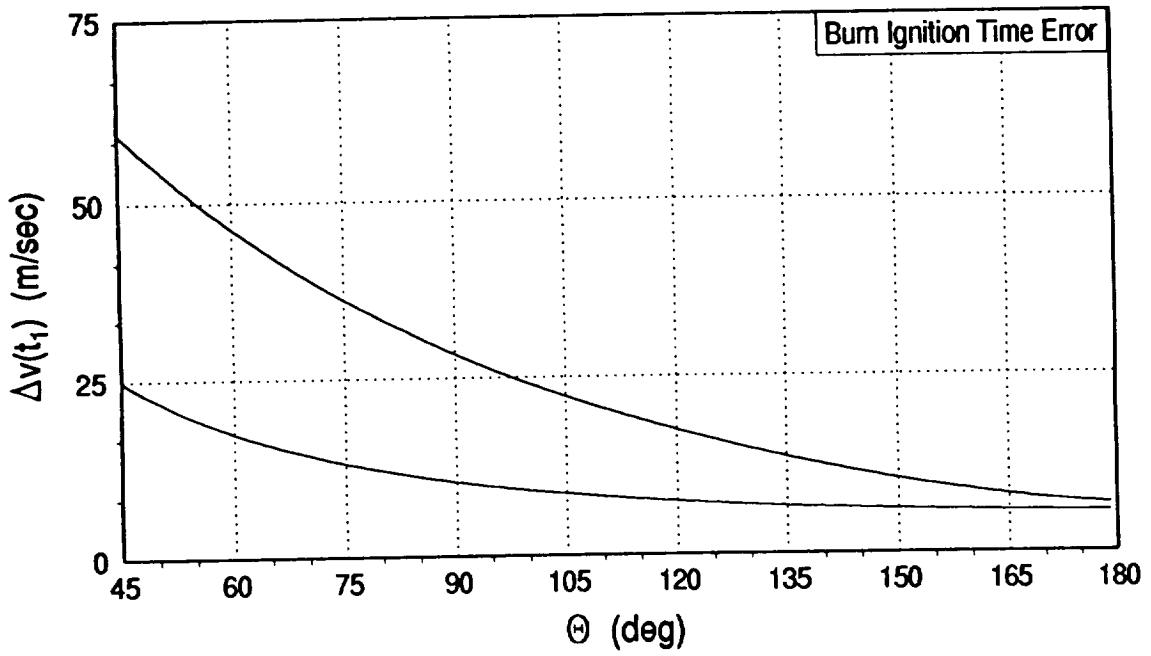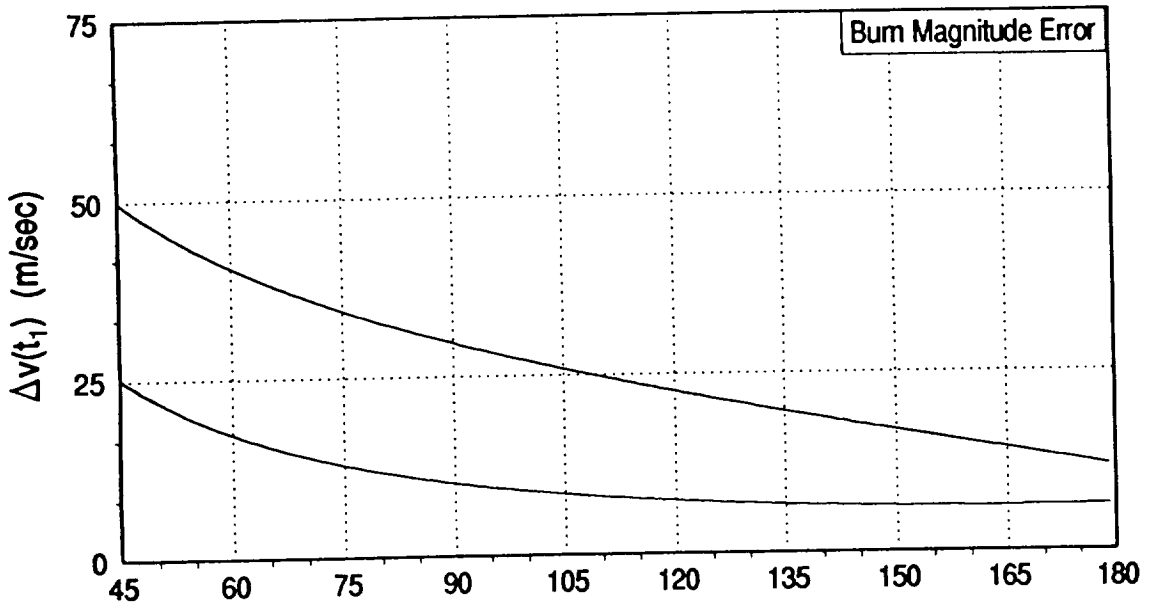
Figure B.2b Closing Velocity - Cocircular Staging Orbit
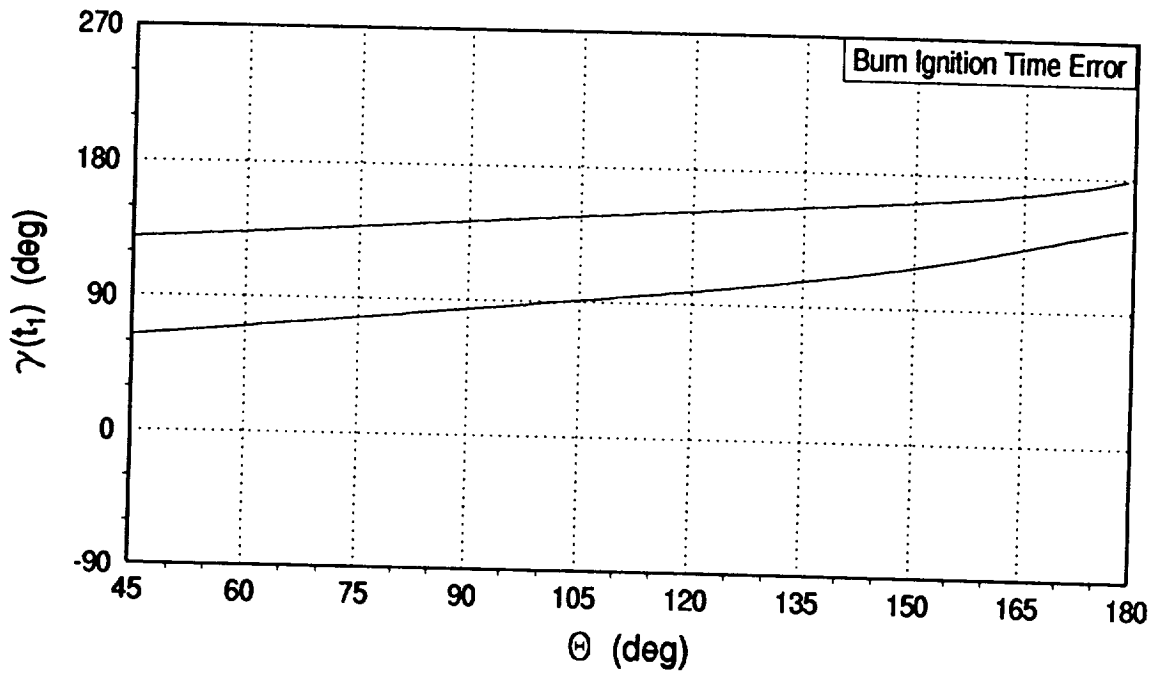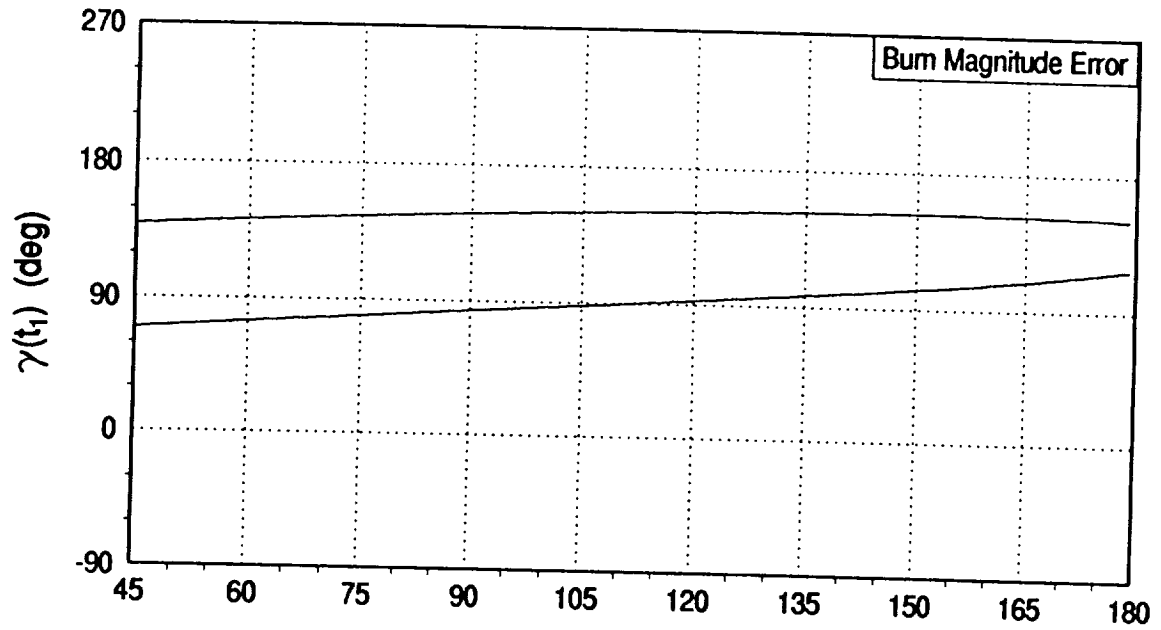
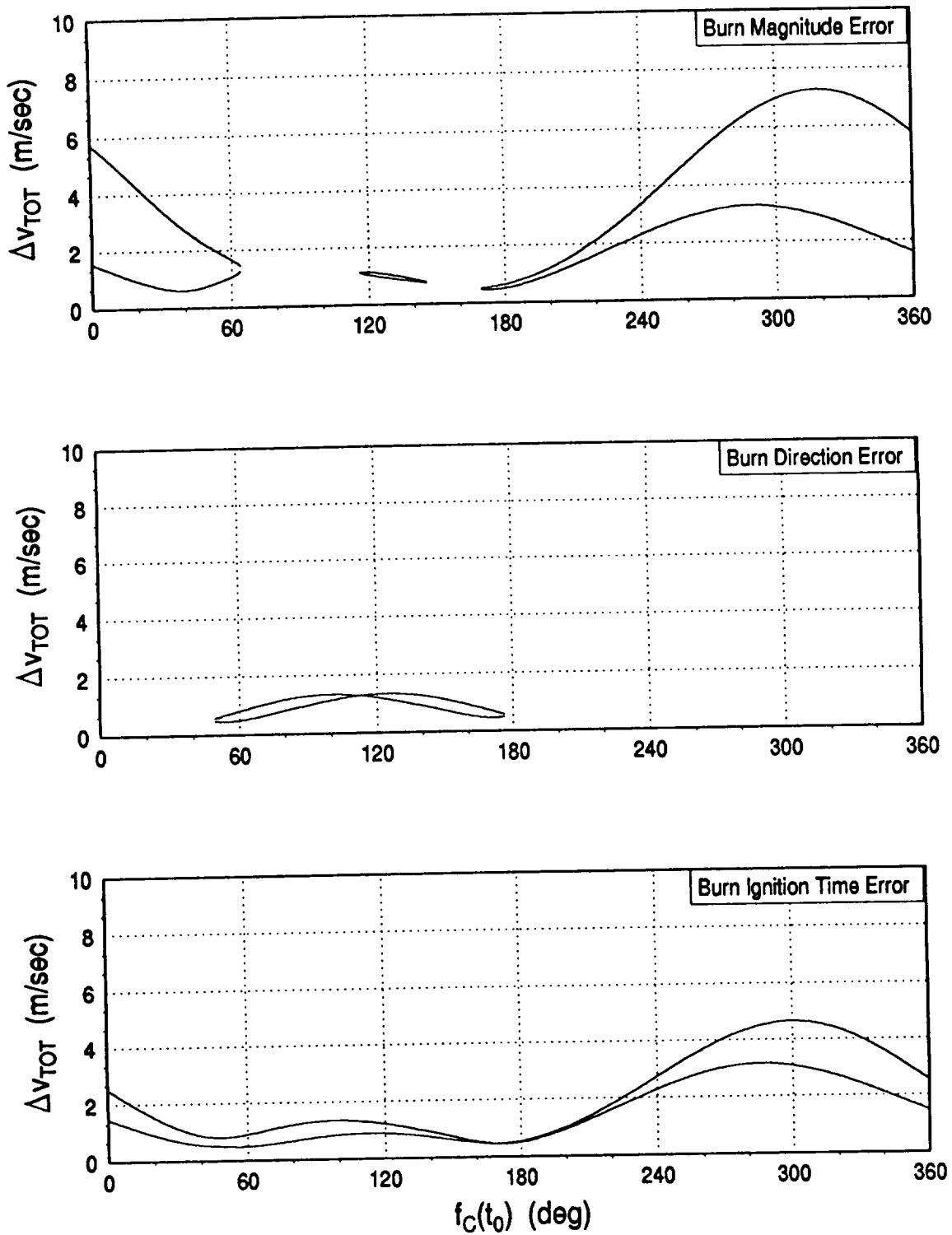Figure B.2c Final Elevation Angle of LOS to Target - Cocircular Staging Orbit

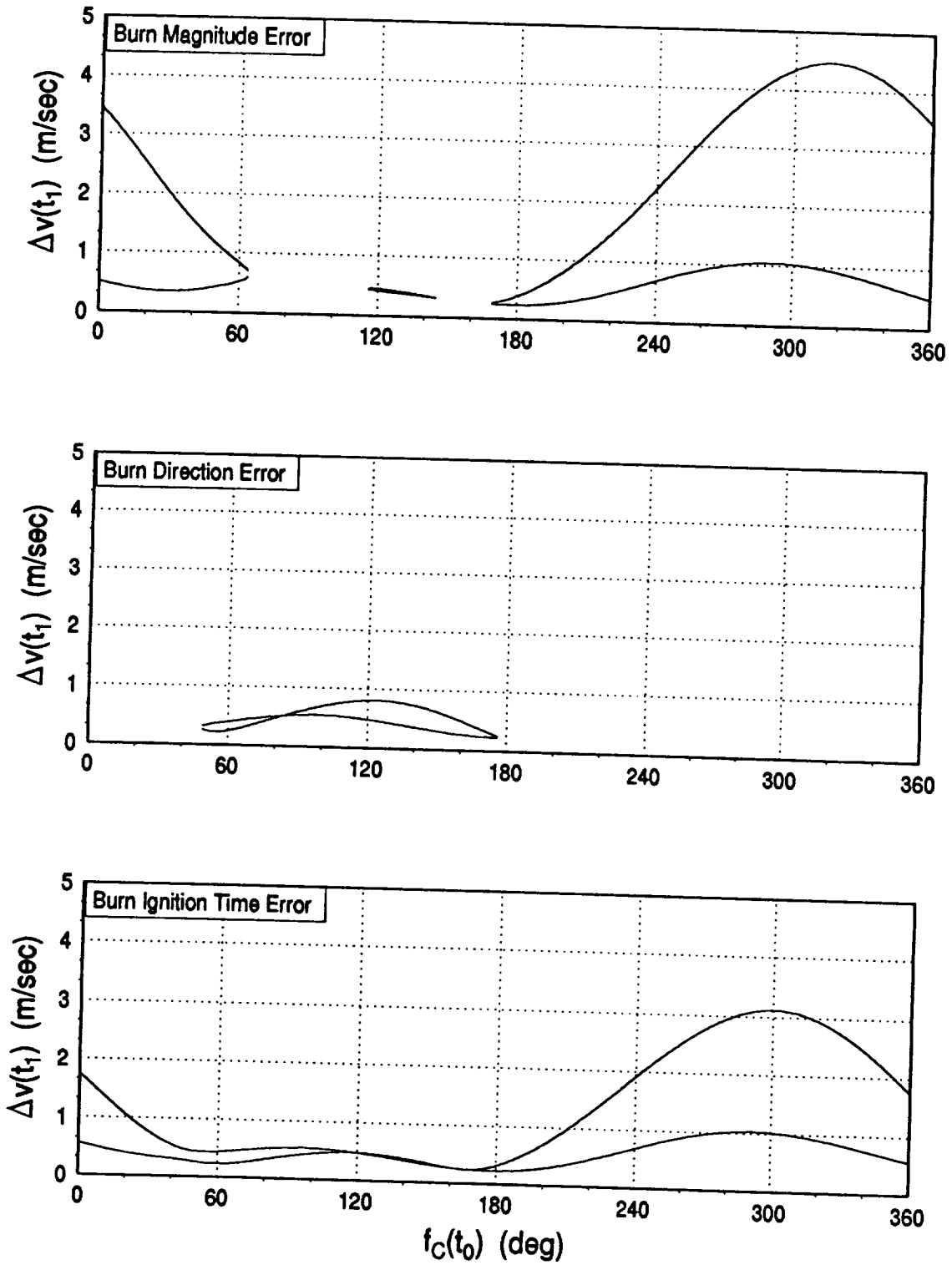Figure B.3a Fuel Expenditure - Scaled Elliptic Staging Orbit

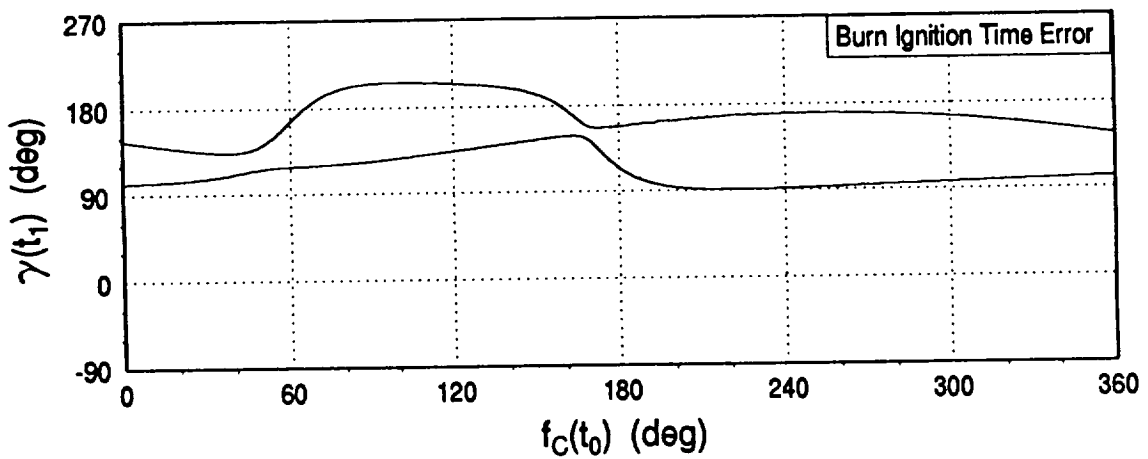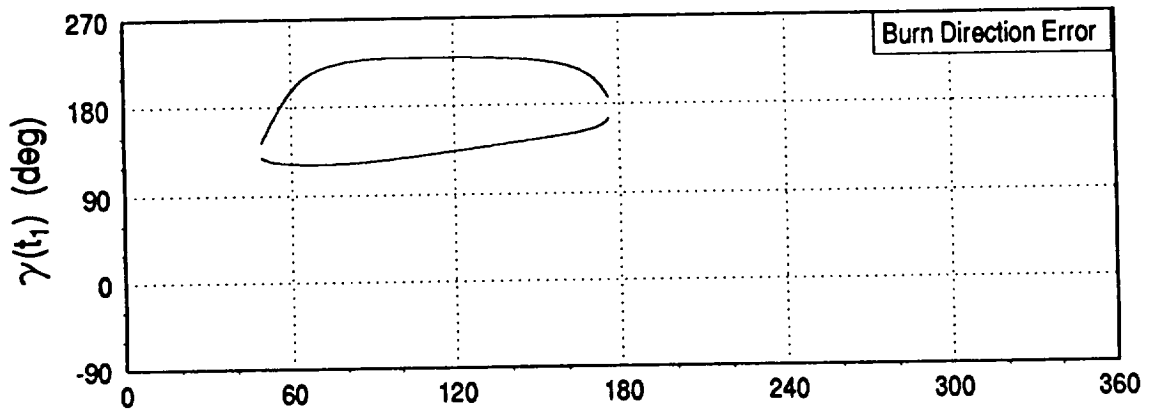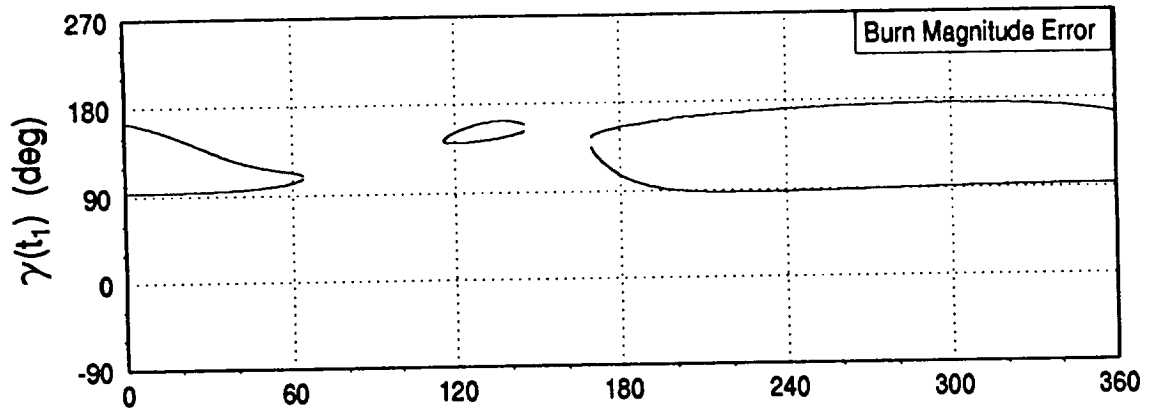Figure B.3b Closing Velocity - Scaled Elliptic Staging Orbit

88

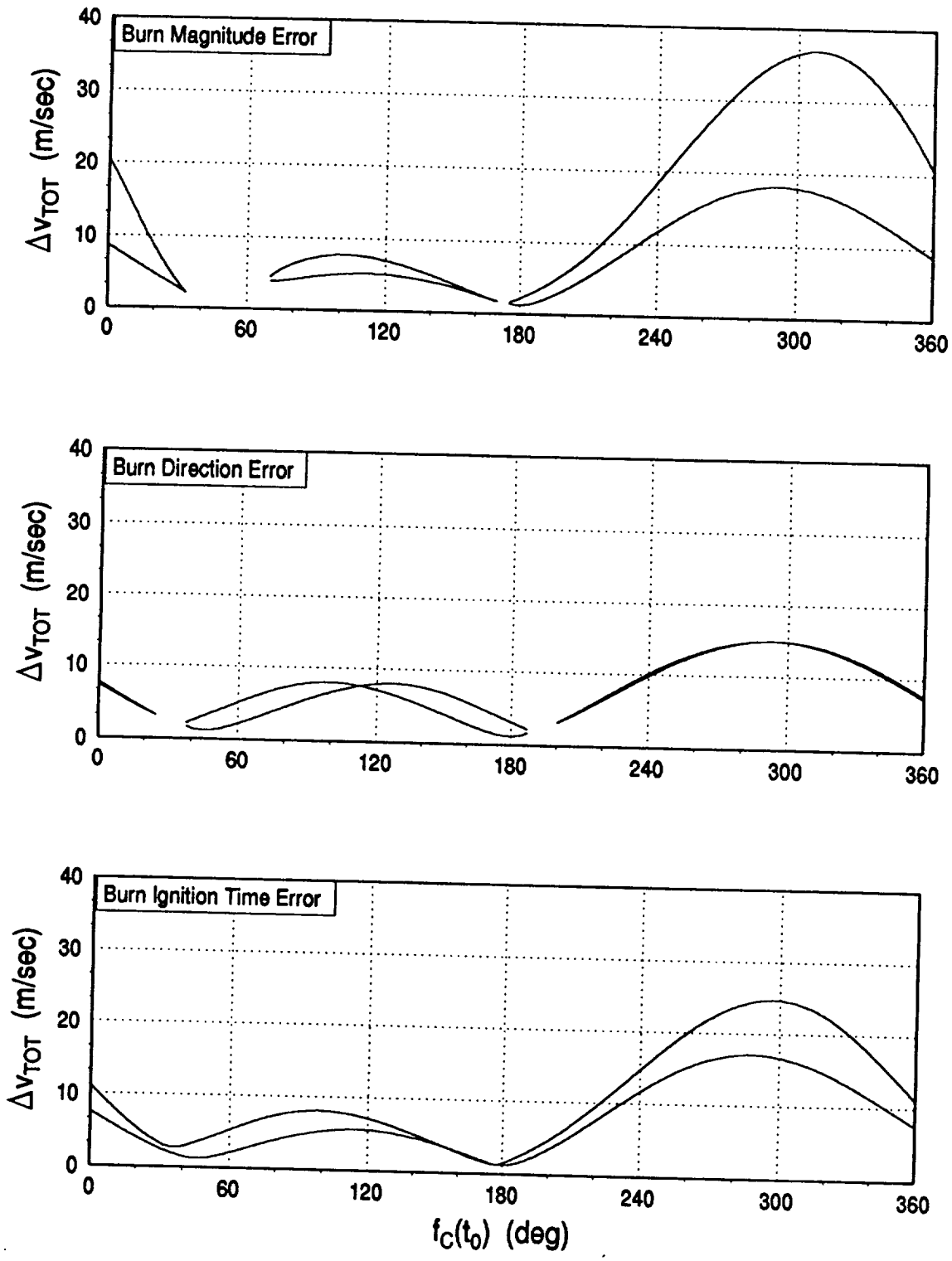Figure B.3c Final Elevation Angle of LOS to Target - Scaled Elliptic Staging Orbit

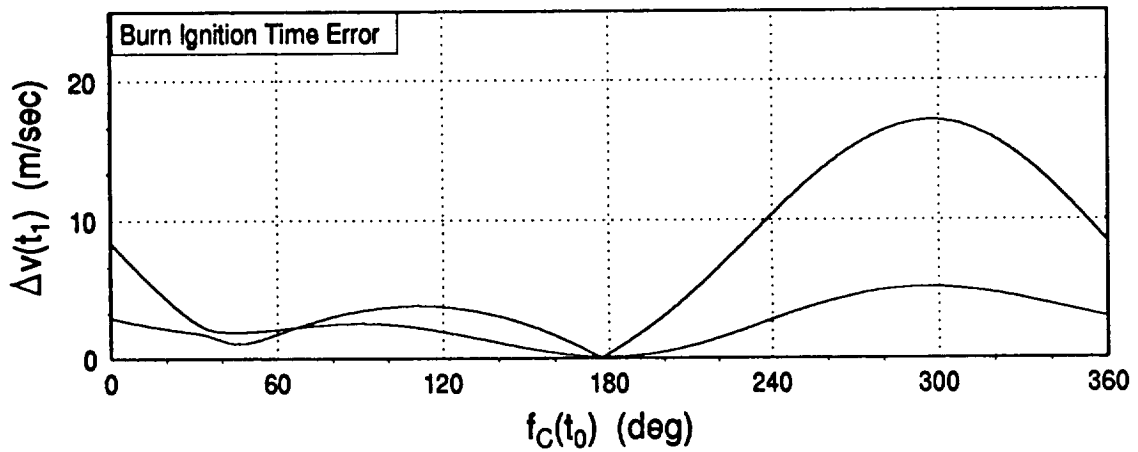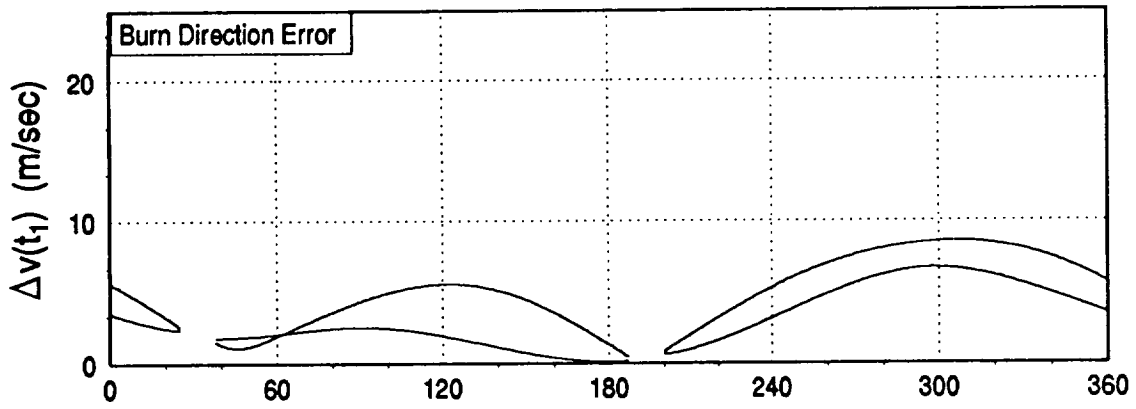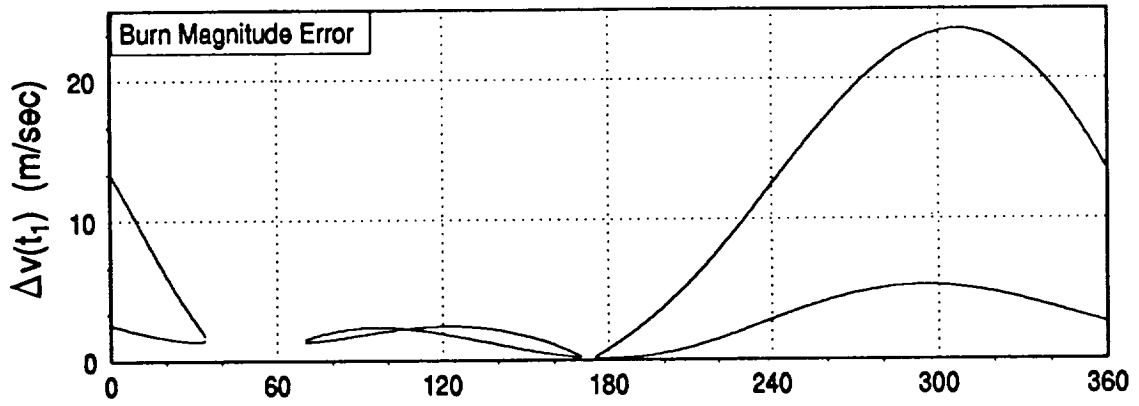Figure B.4a Fuel Expenditure - Coelliptic Staging Orbit

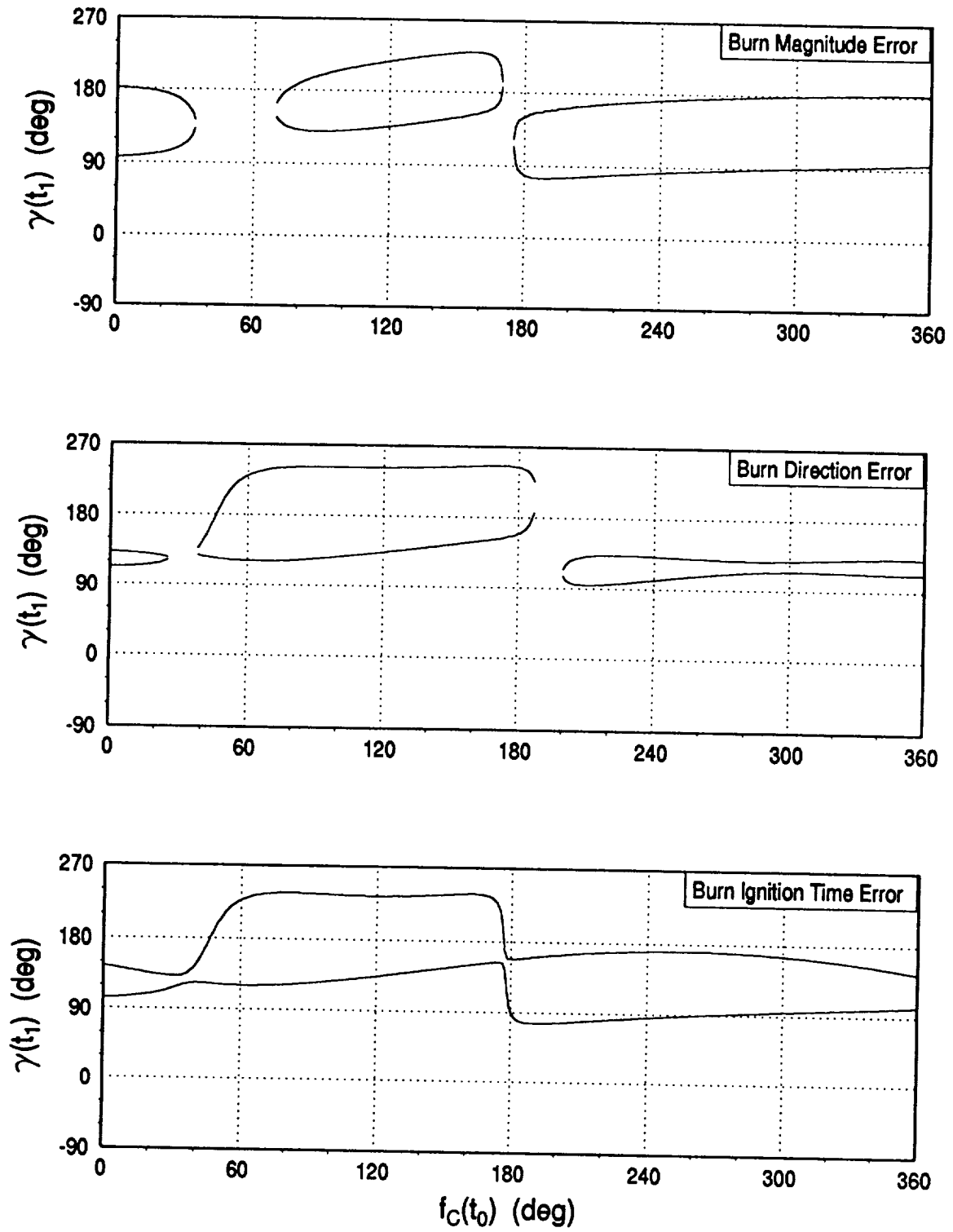Figure B.4b Closing Velocity - Coelliptic Staging Orbit

Figure B.4c Final Elevation Angle of LOS to Target - Coelliptic Staging Orbit

Appendix C

Alternate Solution Sets

This appendix contains two sets of scaled elliptic maneuver points for comparison.

C.1 Alternate Fixed Central Transfer Angle

The first shows the maneuver points providing burn error tolerance for a 90° central transfer angle. Because less time is involved (than for $\Theta = 135°$) these points are grouped much more closely. For larger transfer angles, the region where solutions exist will be larger. A fixed central angle results in different transfer times in different regions of the orbit.

C.2 Fixed Transfer Time

The second set shows the maneuver points providing burn error tolerance for a fixed transfer time of 3/8 of the target's orbital period. Transfers near periapse involve a larger central transfer angle, and those passing through apoapse, a smaller transfer angle. When planning rendezvous with a fixed transfer time, the resulting central transfer angle should be monitored.
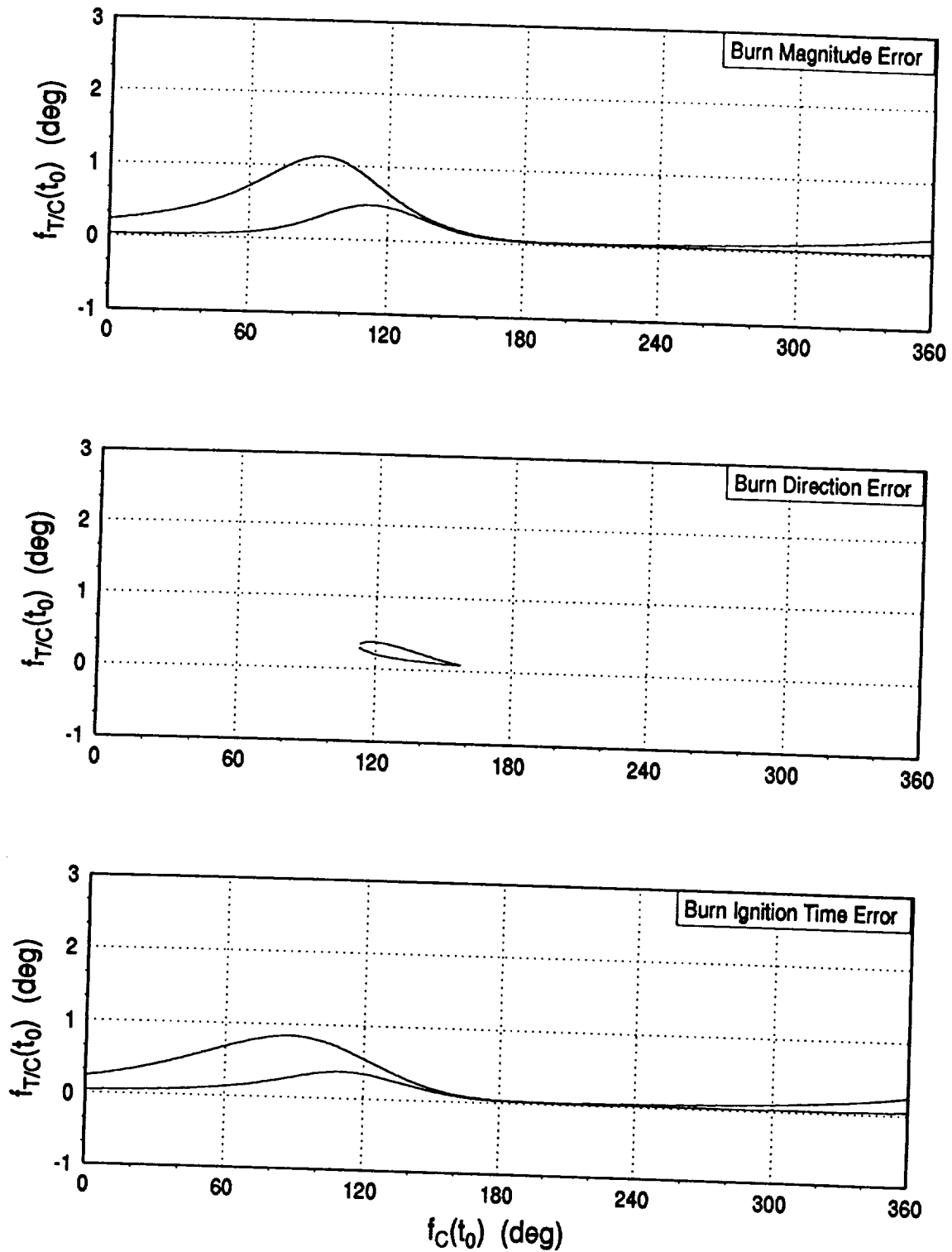
Figure C.1   Maneuver Points Providing Burn Execution Error Tolerance for Scaled
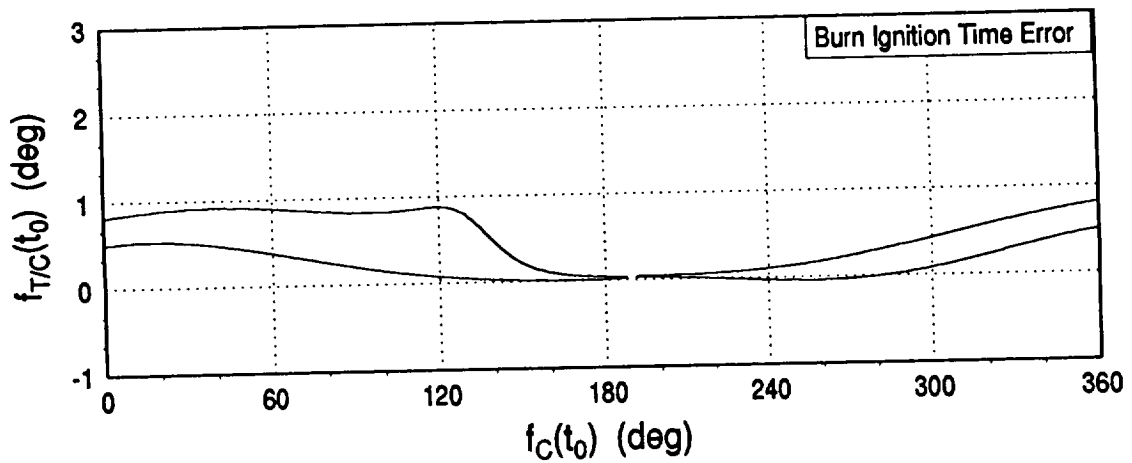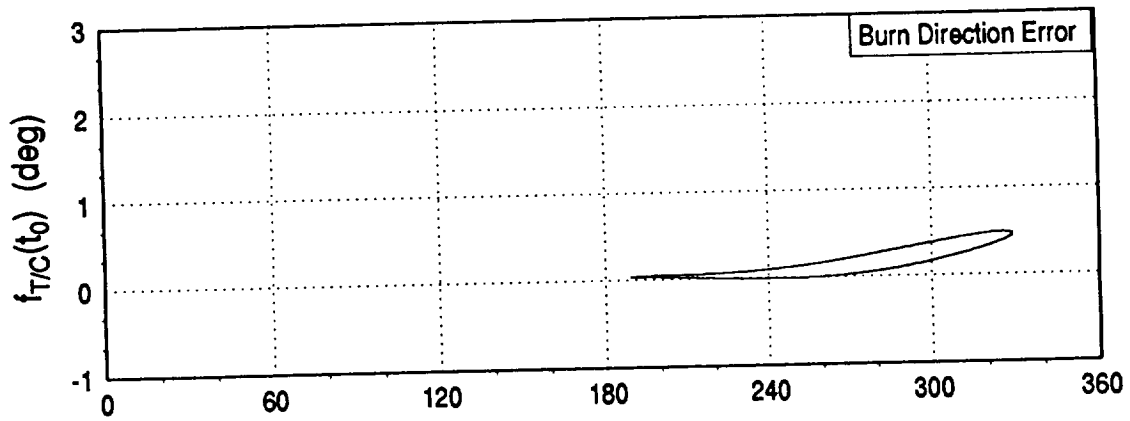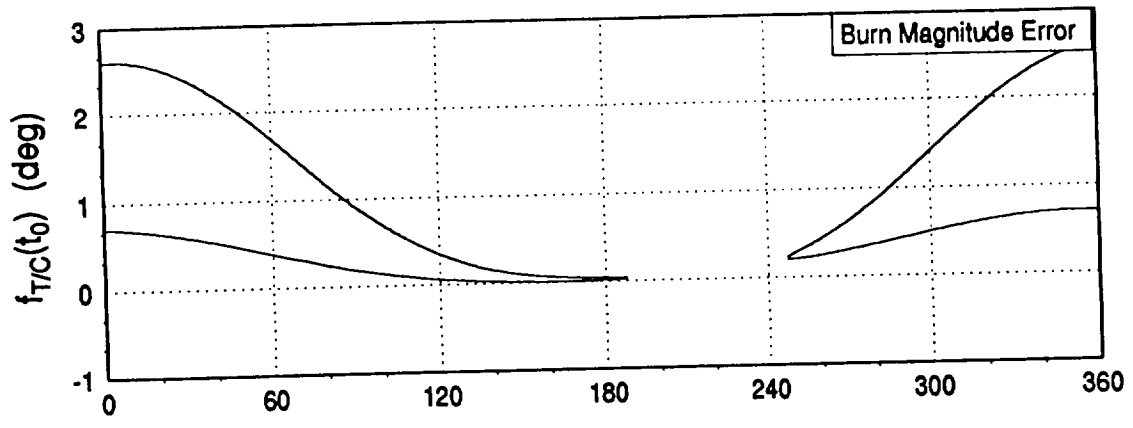Elliptic Staging Orbit and 90° Central Transfer Angle

Figure C.2   Maneuver Points Providing Burn Execution Error Tolerance for Scaled
Elliptic Staging Orbit and Transfer Time = 3/8 P_T

References

1. Battin, R. H., *Introduction to the Mathematics and Methods of Astrodynamics*, American Institute of Aeronautics and Astronautics, Inc., New York, N. Y. 1987.

2. Carter, T. E., "New Form for the Optimal Rendezvous Equations Near a Keplerian Orbit," *Journal of Guidance, Control, and Dynamics*, Vol. 13, No. 1, January-February, 1990.

3. Carter, T. and Humi, M., "Fuel-Optimal Rendezvous Near a Point in General Keplerian Orbit," *Journal of Guidance, Control, and Dynamics*, Vol. 10, Nov.-Dec., 1987, pp. 567-573.

4. Carter, T., "Fuel-Optimal Maneuvers of a Spacecraft Relative to a Point in Circular Orbit," *Journal of Guidance, Control, and Dynamics*, Vol. 7, Nov.-Dec., 1984, pp. 710-716.

5. Chiu, J. -H., "Optimal Multiple-Impuse Nonlinear Orbital Rendezvous," Ph.D. Thesis, University of Illinois at Urbana-Champaign, IL, 1984.

6. Eckel, K. G., "Optimal Impulsive Transfer with Time Constraint," *Astronautica Acta*, Vol. 9, 1982, pp. 139-146.

7. Johnson, M.S., and Giller, D. R., "Apollo Guidance, Navigation, and Control", Vol 5, Massachusetts Institute of Technology, R-700, July 1971.

8. Jones, J. B., "Optimal Rendezvous in the Neighborhood of a Circular Orbit", *The Journal of the Astronautical Sciences*, Vol. 24, Jan .-March 1976, pp. 55-90.

9. Kachmar, P., and Chu, W., "Mars Ascent/Rendezvous Analysis", The C. S. Draper Laboratory, Inc., EGB-90-137, March 1990.

10. Kachmar, P., and Chu, W., "Mars Ascent and Rendezvous Navigation Analysis", The C. S. Draper Laboratory, Inc., EGB-90-327, November 1990.

11. Lawden, D. F., *Optimal Trajectories for Space Navigation*, Butterworths, London, 1963.

12. Prussing, J. E., "Optimal Four-Impulse Fixed-Time Rendezvous in the Vicinity of a Circular Orbit," *American Institute of Aeronautics and Astronautics Journal*, Vol. 7, May 1969, pp. 928-935.

13. Prussing, J. E., "Optimal Two- and Three-Impulse Fixed-Time Rendezvous in the Vicinity of a Circular Orbit", *American Institute of Aeronautics and Astronautics Journal*, Vol. 8, July 1970, pp. 1221-1228.

14. Prussing, J. E. and Chiu, J. -H., "Optimal Multiple-Impulse Time-Fixed Rendezvous Between Circular Orbits," *Journal of Guidance, Control, and Dynamics*, Vol. 9, No. 1, January-February, 1986.

15. Shepperd, S. W., "Elliptic Orbit Rendezvous - Issues and Preliminary Results", The C. S. Draper Laboratory, Inc., EGB-90-162, March 1990.

16. Tschauner, J., "Elliptic Orbit Rendezvous," *AIAA Journal*, Vol. 5, No. 6, 1967, pp. 1110-1113.